Modifed Colloidal Primitive Model as a Homogeneous Surface Charge Distribution: ζ-Potential.

ARTICLE *in* THE JOURNAL OF PHYSICAL CHEMISTRY B · AUGUST 2013

Impact Factor: 3.3 · DOI: 10.1021/jp403313k · Source: PubMed

2 AUTHORS:

Manzanilla Granados
Instituto Politécnico Nacional
4 PUBLICATIONS **22** CITATIONS
SEE PROFILE

Marcelo Lozada-Cassou
Universidad Nacional Autónoma de México
118 PUBLICATIONS **2,481** CITATIONS
SEE PROFILE

THE JOURNAL OF PHYSICAL CHEMISTRY B

Article

pubs.acs.org/JPCB

Modified Colloidal Primitive Model as a Homogeneous Surface Charge Distribution: ζ-Potential

Héctor M. Manzanilla-Granados[†] and Marcelo Lozada-Cassou*[,‡]

[†]Escuela Superior de Computo, Instituto Politécnico Nacional, U. P. Adolfo López Mateos, Ciudad de México, 07738, México

[‡]Programa de Ingeniería Molecular, Instituto Mexicano del Petróleo, Col. San Bartolo Atepehuacan C.P., Ciudad de Mexico, 07730, México

ABSTRACT: An integral equations theory is derived and applied to a modified colloidal primitive model (MCPM), for finite concentration colloidal dispersions. In MCPM, the charge on the colloidal particle is assumed to be smeared on its surface. We find important quantitative and qualitative differences of the ζ-potential, induced charge, and the colloid−colloid electric effective force, calculated in the MCPM, with those obtained from the colloidal primitive model (CPM), where the colloidal charge is assumed to be in the center of the particle, in spite of the fact that, due to Gauss's law, both models have *the same particle distribution function*. In particular, for the same parameters, while the ζ-potential is positive in MCPM, is negative in the CPM, implying opposite electrophoretic mobilities, μ. An inverse μ has been theoretically predicted in the past, for infinite dilution colloidal dispersions. The MCPM could be a better model for some colloidal particles. In both models, the CPM and the MCPM, it is found a very long-range colloid−colloid correlation, in accordance with previous Monte Carlo simulations. The electrostatic, as well as entropic, like-charged colloid−colloid forces are oscillatory, implying a long-range attraction.

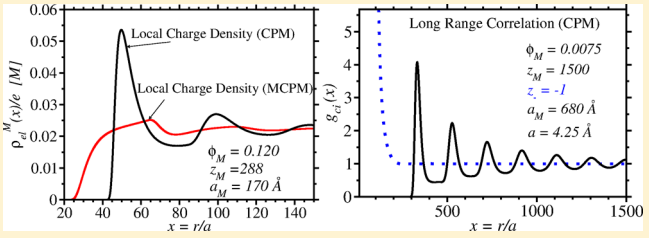

1. INTRODUCTION

At the center of theoretical studies of colloidal dispersions is the understanding of their stability conditions, i.e., the study of the many-body colloid−colloid effective force. For the case of charged colloids, it has been long recognized that the electrolyte structure surrounding the colloidal particles, the so-called electrical double layer (EDL), plays a most relevant role. First studies were for a point ion model (PIM) electrolyte solution, next to an external field produced by only one or two colloidal particles. In this approach, the ions are punctual particles, with charge q_i, the solvent is a uniform dielectric medium, with a constant dielectric constant, ε, and the colloid particles are large, charged particles, of different simple geometries, at *infinite dilution*, and such that their dielectric constant is equal to that of the solvent, to neglect image charges of the ions. The system was solved through the Poisson−Boltzmann (PB) equation, i.e., the Derjaguin−Landau−Verwey−Overbeek (DLVO) theory.[1] One of the predictions of the DLVO theory is the monotonic behavior of EDL, for different geometries of the colloidal particles, as well as a monotonic repulsive force between two, like-charged, colloidal particles. An improvement to the PIM is to consider the hydrated ionic size. Such model is the restricted primitive model (RPM),[2,3] which considers the ionic species as spherical hard ions, all of same size, with charge at its center. To study the EDL of the RPM, next to a model colloidal particle, various Monte Carlo (MC) and molecular dynamics (MD) computer simulations were made,[4−6] and powerful many-body liquid theories were developed: (a) hierarchy equations, such as the Stillinger−Kirkwood,[7] and Born−Green−Yvon;[8] (b) modified Poisson−Boltzmann;[9,10] (c) density functional;[11−13] and (d) integral equations.[2,6,14−22] In particular, we have developed, and successfully applied, the hypernetted chain/mean spherical approximation (HNC/MSA) integral equation to different systems.[21,22]

Computer simulations and many-body liquid theories studies of the RPM, next to a single charged colloidal particle or between two charged colloidal particles, show an oscillatory EDL.[4,5,17,18,21−28] These oscillations imply new phenomena, such as charge reversal, and charge inversion, as an effect of the overcompensation of charge around the electrode.[4,24,25,29−31] These new phenomena were able to explain in an indirect way experimental observations, such as the inversion of the electrophoretic mobility, μ,[23,32−46] and the attraction between like-charged colloids,[6,12,14,15,18,24,27,47−53] which could not be explained by ionic punctual models. Several improvements to the RPM, were developed to have more realistic models. For example, ionic size asymmetry, was considered.[28,30,54] This model is known as the primitive model (PM). A colloidal particle immersed in a PM results in new phenomena, such as *surface charge amplification* (SCA),[55−58] also referred to as *true overcharging*,[59] and was found a new relevant role of the co-ions in the EDL,[28,55,56,60] where the SCA results from an excess of adsorbed co-ions on the electrode surface, associated to the

Received: April 3, 2013
Revised: July 6, 2013
Published: August 19, 2013

   dx.doi.org/10.1021/jp403313k | *J. Phys. Chem. B* 2013, 117, 11812−11829

adsorbed, larger, counterions. This SCA promotes an excess of contiguous opposite charge (charge reversal), which is responsible for another contiguous layer (with the same sign of co-ions) resulting as a charge inversion. These phenomena result from the stratification of the EDL, and has been explained satisfactorily by means of energy-entropy balance mechanisms.[28,55,56,60] With SCA, the otherwise standard charge reversal and charge inversion[4,12,23,49,61] are enhanced.

If, in the PM, in addition to the electrolyte, we consider large, charged particles, at *finite concentration*, we have a model for a colloidal dispersion. We refer to this model as colloidal primitive model (CPM). Recently we have applied the HNC/MSA theory to the CPM.[62,63] In the PM, and, hence, in the CPM, the particles are taken as charged, hard spheres, with their charge in their centers. Our HNC/MSA results for the CPM show a high stratification of the EDL, which is responsible for magnifying phenomena such as a SCA, charge reversal, and charge inversion, and the appearance of polarity inversion of ζ-potential. In particular, it is shown that the widely used cell model,[64−66] for finite concentration colloids, is quantitatively and qualitatively in disagreement with the CPM,[62] while the CPM is in agreement with molecular dynamics simulations.[63]

As pointed out above, in the CPM, the charge of the colloidal particle is assumed to be in its center. However, other possibilities are to assume it to be discretely distributed, or spread, on its surface. Computer simulation comparisons of the EDL's of a single colloidal particle, with its charge discretely distributed or with central charge, have been made by Le Bret, since 1984;[67] since then, other studies have been made, for example by Messina.[68] The main conclusion is that, the difference is negligible for most cases of interest. It should be pointed out, however, that in this implicit cell model of a colloidal dispersion, no interaction of the colloidal particles is considered, and the ionic sizes are of model hydrated ions.[69,70] For the interaction of charged surfaces, however, the charge distribution does matter.[71]

If one applies Gauss' law to a central colloidal particle, with its charge in its center, or on its surface, the electrical field is, of course, the same. Hence, in the many-body theory of liquids, integral equations, such as the HNC/MSA, are identical for both models, and so it is the potential of mean force and the concentration profiles. However, this does not have to be the case for the mean electrostatic potential, since, for the electrostatic potential, the charge location does matter. Hence, in this paper we study a modified colloidal primitive model (MCPM), which differs from the CPM only in that the colloidal charge is uniformly smeared on the their surfaces. We calculate various colloidal charge dependent quantities, such as the ζ-potential and induced charge, and its implications for the μ. We also address to the problem of like-charge colloid−colloid attraction, at finite colloidal concentration.

THEORY

Integral Equations for Homogeneous and Inhomogeneous Colloidal Dispersions. The multicomponent Ornstein−Zernike equations for an homogeneous fluid of $n + 1$ species are

$$h_{ij}(\mathbf{r}_{12}) = c_{ij}(\mathbf{r}_{12}) + \sum_{l=1}^{n+1} \rho_l \int_V h_{il}(\mathbf{r}_{13}) c_{lj}(\mathbf{r}_{23}) d\mathbf{r}_3 \tag{1}$$

where $i,j = 1, 2, ..., n+1$, ρ_l is the number density of species l, $h_{ij} \equiv g_{ij}(\mathbf{r}_{12}) - 1$, and $c_{ij}(\mathbf{r}_{12})$, are the total and direct correlation functions, respectively, for particles 1 and 2, of species i and j, with position vectors $\mathbf{r}_1$ and $\mathbf{r}_2$, respectively. $g_{ij}(\mathbf{r}_{12})$ is the radial distribution function, and $\mathbf{r}_{12} = \mathbf{r}_2 - \mathbf{r}_1$. To solve eqs 1, we employ two different closures approximations for $c_{ij}(\mathbf{r}_{21})$, i.e, the hypernetted-chain (HNC)

$$c_{ij}(\mathbf{r}_{12}) = h_{ij}(\mathbf{r}_{12}) + \beta u_{ij}(\mathbf{r}_{12}) - \ln g_{ij}(\mathbf{r}_{12}) \tag{2}$$

in the first right-hand side term of eqs 1, and the mean spherical approximation (MSA)

$$c_{ij}(\mathbf{r}_{12}) = -\beta u_{ij}(\mathbf{r}_{12}) \tag{3}$$

in the convolution integral. In eqs 2 and 3, $\beta \equiv 1/k_B T$, k_B being the Boltzmann constant, and T the absolute temperature. u_{ij}, is the direct electrostatic potential, i.e.,

$$u_{ij}(r) = \begin{cases} \infty & \text{for } r < a_{ij} \\ \dfrac{q_i q_j}{\varepsilon r} & \text{for } r \geq a_{ij} \end{cases}, \quad \text{with } i, j = 1, ..., n+1 \tag{4}$$

where r is the particles distance, $a_{ij} = (a_i + a_j)/2$, and a_i is the diameter of species i. Equations 1 together with eqs 2 and 3 are the HNC/MSA integral equations for an homogeneous fluid. For an $n+1$ species (homogeneous fluid), eqs 1 become a system of $(n + 1)^2$ coupled integral equations. However, taking into account that $h_{ij}(\mathbf{r}_{12}) = h_{ji}(\mathbf{r}_{12})$, the total number of equations is reduced by $n(n + 1)/2$, and we end with $(n + 1)(n + 2)/2$ independent, coupled, integral equations.

Using the fact that particles and fields are equivalent, it has been shown[15,21,32,72] that many-body correlations (inhomogeneous fluids equations) can be obtain directly from equations for homogeneous fluids, by simply considering one of the species in the fluid, at zero concentration, as the source of the external field. Hence, choosing the species $(n + 1)$, as a the source of an external field, renaming it as $\gamma \equiv n + 1$, and taking $\rho_\gamma \to 0$, eqs 1 become

$$h_{ij}(\mathbf{r}_{12}) = c_{ij}(\mathbf{r}_{12}) + \sum_{l=1}^{n} \rho_l \int_V h_{il}(\mathbf{r}_{13}) c_{lj}(\mathbf{r}_{23}) d\mathbf{r}_3 \tag{5}$$

with $i,j = 1, 2, ..., n, \gamma$, and where the summation over the convolution now runs only up to n, and we have $(n + 1)^2 - 1$ equations. However, considering the symmetry relation $h_{ij}(\mathbf{r}_{12}) = h_{ji}(\mathbf{r}_{12})$, the total number of equations is reduced by $n(n+1)/2$, and we end with $(n + 1)(n + 2)/2 - 1$ independent, coupled, integral equations, of which $n(n + 1)/2$ equations correspond to the bulk, i.e., away from the external field:

$$h_{ij}(\mathbf{r}_{12}) = c_{ij}(\mathbf{r}_{12}) + \sum_{l=1}^{n} \rho_l \int_V h_{il}(\mathbf{r}_{13}) c_{lj}(\mathbf{r}_{23}) d\mathbf{r}_3, \quad \text{for } i, j = 1, ..., n \tag{6}$$

and n equations are for the inhomogeneous part, i.e., for the fluid structure close to the external field:

$$h_{\gamma j}(\mathbf{r}_{12}) = c_{\gamma j}(\mathbf{r}_{12}) + \sum_{l=1}^{n} \rho_l \int_V h_{\gamma l}(\mathbf{r}_{13}) c_{lj}(\mathbf{r}_{23}) d\mathbf{r}_3 \quad \text{for } i, j = 1, ..., n, \gamma \tag{7}$$

where we have taken into account that, at infinite dilution of the γ-species, $h_{\gamma\gamma}(\mathbf{r}_{12}) = 0$.

If in the bulk equations (eq 6), the MSA approximation for the direct correlation function, $c_{ij}(\mathbf{r}_{21})$, is used in *both* the first term of its right-hand side and in the convolution integral, they can be analytically solved.[73−75] We will use this approach in this paper. Other approximations and/or combinations for $c_{ij}(\mathbf{r}_{21})$, in eq 6, are of course possible.[21] We will not discuss them here. For the inhomogeneous equations (eq 7) we use the HNC closure, for the $c_{\gamma j}(\mathbf{r}_{21})$, in the first term of its right-hand side, but the MSA closure for $c_{ij}(\mathbf{r}_{23})$ in the convolution integral. Notice that the MSA direct correlation functions, $c_{ij}(\mathbf{r}_{23})$, in the convolution integral of eq 7, are obtained from eq 6. The total $(n + 1)^2 - 1$ equations can be numerically solved with finite elements numerical methods.[76,77] We refer to this system of coupled, nonlinear integral equations (eqs 6 and 7) as the HNC/MSA inhomogeneous equations for n-species next to an external field, and to eq 1, together with the HNC and MSA approximations (eqs 2 and 3) as the HNC/MSA homogeneous equations for $(n + 1)$ species. The homogeneous and inhomogeneous HNC/MSA equations have been solved in the past for homogeneous and inhomogeneous RPM[6,12,21,22] and PM[28,30,60] electrolyte solutions, with good agreement with computer simulations, and for inhomogeneous,[55,78] and homogeneous[62,63] CPM, finite concentration, colloidal dispersions.

As pointed out above, using the equivalence between particles and fields, one can readily obtain integral equations for inhomogeneous fluids from homogeneous fluids equations, by assuming one of the species to be at infinite dilution, and as the source of the external field. The contrary is also true: one can derive homogeneous fluid integral equations from inhomogeneous fluids equations by assuming that the external field is just another particle of the fluid.[15,21,32,72,79] In this work we use this second approach to derive integral equations for an homogeneous colloidal suspension.

While our formalism can be applied to any number of species (for homogeneous or inhomogeneous fluids) next to an external field of any geometry, in this work we present the detailed algebra for four species in an external field of spherical geometry, derive the corresponding homogeneous equations, and present numerical results only for one species, *homogeneous*, colloidal dispersion, immersed in a two-species RPM electrolyte. We leave the general case of related interesting systems for forthcoming publications.

The Models. We study two models, the colloidal primitive model (CPM) and the modified colloidal primitive model (MCPM). The first (see Figure 1a) is an extension of the PM, i.e., the ions and colloidal particles are spherical hard particles with charge in their centers. The colloidal particles' counterions are taken as another PM species. Their size and charge can or

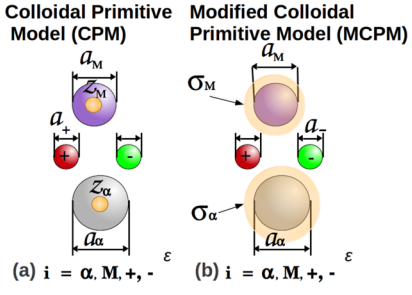

Figure 1. (a) Schematic representation of the CPM and (b) the MCPM with its charged smeared over its surface.

can not be equal to that of one of the salt ions species. All particles are immersed in a continuum medium with dielectric constant ε. A modification of the CPM is that in which the charge of the colloidal particle is uniformly smeared over its surface, while everything else remains unchanged. We refer to this other model as the modified colloidal primitive model (MCPM) (see Figure 1b). The charges of the little ions are located in their centers.

Thus, in general, we have five species: one corresponds to the external field, labeled by $i = \gamma$, which, as pointed out above, can be taken as a central spherical particle, say a nanoparticle, at infinite dilution $(\rho_\gamma \to 0)$; another corresponds to macroions labeled by $i = M$; another two for the anions and cations of an added salt, labeled by signs $i = -$ and $i = +$, respectively; and one corresponding to the colloidal particles' counterions $i = c$. We define z_γ and a_γ, as the valence and diameter of the central nanoparticle, respectively. With respect to the central nanoparticle, the colloidal dispersion is an inhomogeneous fluid. For the CPM, the species' valences and diameters are z_i and a_i, with $i = M, +, -, c$, while in MCPM, we denote the colloid's valence by its equivalent surface charge density σ_M, i.e., $\sigma_M = z_M e/\pi a_M^2$ where e corresponds to the elemental proton charge. In both models, the species number densities are ρ_i.

The *unscreened* interaction potential, $u_{ij}(r)$, between two particles of species i and j, separated by a distance $r \equiv |\mathbf{r}_{12}|$, is

$$u_{ij}(r) = \begin{cases} \infty & \text{for } r < a_{ij} \\ \dfrac{q_i q_j}{\varepsilon r} & \text{for } r \geq a_{ij} \end{cases} \quad \text{with } i, j = M, +, - \tag{8}$$

where $a_{ij} = (a_i + a_j)/2$, and $q_i = ez_i$. For CPM, $q_M = ez_M$, while for the MCPM, $q_M = \pi a_M^2 \sigma_M$. Of course, in both models, $u_{ij}(r)$ takes the same values for a given q_M (Gauss law). This is also true for the direct interaction potential, $u_{\gamma i}(r)$, between the central particle γ and any other species i in the fluid, i.e.,

$$u_i(r) = \begin{cases} \infty & \text{for } r < a_{\gamma i} \\ (q_\gamma q_i)/\varepsilon r & \text{for } r \geq a_{\gamma i} \end{cases} \quad \text{with } i = M, +, -, c \tag{9}$$

where hereinafter we omit the subindex γ, for notation simplicity, i.e., $u_i(r) \equiv u_{\gamma i}(r)$. With these interaction potentials, adequately substituted in eqs 2 and 3, together with eqs 6 and 7, one can compute the HNC/MSA inhomogeneous radial distribution functions, $g_i(r) \equiv g_{\gamma i}(r)$, the potential of mean force, $w_i(r) \equiv w_{\gamma i}(r)$, mean electrostatic potential, $\psi(r) \equiv \psi_\gamma(r)$, and the induced charge density, $\sigma(r) \equiv \sigma_\gamma(r)$, profiles, as a function of the distance, r, to the central nanoparticle, and the electrostatic, $F_{ei}(r) \equiv F_{e\gamma i}(r)$, and entropic, $F_{si}(r) \equiv F_{s\gamma i}(r)$, components of the mean force, $F_{wi}(r) \equiv F_{w\gamma i}(r) \equiv -\mathrm{d}(w_j(r))/\mathrm{d}r$, between the central nanoparticle of species γ and a particle of species i at a distance r in the fluid. All these quantities can be calculated for either the CPM or MCPM. However, as we mentioned above, in this paper we will present calculations only for the homogeneous CPM and MCPM.

To explicitly obtain the inhomogeneous HNC/MSA integral equations a CPM or MCPM around an external field of spherical geometry (central particle of species γ), see Figure 2, we first define the parameters $t \equiv |\mathbf{t}|$ and $s \equiv |\mathbf{s}|$, where $\mathbf{s} \equiv \mathbf{r}_{23}$ and $\mathbf{t} \equiv \mathbf{r}_{13}$. Analytically solving eq 6, with eqs 3 and 8, the MSA expressions for $c_{ij}(s)$ of the homogeneous CPM or MCPM can obtained[73−75] and expressed as

dx.doi.org/10.1021/jp403313k | J. Phys. Chem. B 2013, 117, 11812−11829

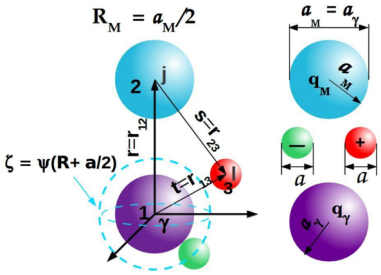

Figure 2. Schematic representation of a fluid of four species.

$$c_{lj}(s) = c_{lj}^{sr}(s) + c_{lj}^{hs}(s) - \frac{\beta q_l q_j}{\varepsilon s} \tag{10}$$

where $c_{lj}^{sr}(s)$ corresponds to the short-range correlations due to electrostatic interactions, whereas $c_{lj}^{sr}(s)$ corresponds to short-range correlations associated with the hard-sphere interactions. The analytic expressions for these functions are given in Appendix A. The volume element $d\mathbf{r}_3$, in terms of s, t, and ϕ, is expressed as $d\mathbf{r}_3 = (st/r)\, ds\, dt\, d\phi$. Hence, substituting eq 10 in the convolution integral of eq 7 and the HNC closure, eq 2, on the first right-hand side of eq 7, we get

$$g_j(r) = \exp\{-\beta q_j \psi(r) + 2\pi A_j(r) + 2\pi \sum_{l=M,+,-,c} \rho_l \int_{a_{Ml}}^{\infty} h_l(t)[K_{lj}(r, t) + L_{lj}(r, t)]t\, dt\} \tag{11}$$

such that $j = M, +, -, c$, and $\psi(r)$ is the mean electrostatic potential (see Appendix B), given by

$$\psi(r) = \frac{u_{\gamma j}(r)}{q_j} - \frac{2\pi}{\varepsilon r} \sum_{l=M,+,-,c} \int_{a_{Ml}}^{\infty} q_l \rho_l h_l(t) f_1(r, t)t\, dt \tag{12}$$

where we define, $f_1(r,t) \equiv -[r + t - |r - t|]$. This equation can also be expressed as

$$\psi(r) = \frac{4\pi}{\varepsilon} \int_r^{\infty} \rho_{el}(y)\left(y - \frac{y^2}{r}\right) dy \tag{13}$$

where $\rho_{el}(y)$ is the local charge concentration profile, given by

$$\rho_{el}(y) = \sum_{j=M,+,-,c} q_j \rho_j g_j(y) \tag{14}$$

Equations 13 and 14 are general results that are independent of the charge distribution on the colloidal particles (see eqs 103 and 106 in Appendix B).

To obtain eqs 11, we have used the fact that the fluid is electroneutral, i.e.,

$$\sum_{i=M,+,-,c} z_i e \rho_i = 0 \tag{15}$$

The term $A_j(r)$, from eq 11, is given by

$$A_j = \sum_{l=M,+,-,c} \rho_l \int_0^{a_{\gamma l}} h_{\gamma l}(t)[L_{lj}(r, t) + K_{lj}(r, t)]t\, dt \tag{16}$$

where, $L_{lj}(r,t)$ and $K_{lj}(r,t)$ are analytical expressions, given in Appendix A (see eqs 56 and 57). Defining $J_j(r)$ as

$$J_j(r) \equiv -2\pi k_B T A_j(r) - 2\pi k_B T \sum_{l=M,+,-,c} \rho_l \int_{a_{Ml}}^{\infty} h_l(t)[K_{lj}(r, t) + L_{lj}(r, t)]t\, dt \tag{17}$$

Equation 11 becomes

$$g_j(r) = \exp\{-\beta[q_j \psi(r) + J_j(r)]\} \tag{18}$$

Equations 11 or 18 are the HNC/MSA equations for a colloidal dispersion, next to an external field of spherical geometry, represented by species γ, at infinite dilution. The potential of mean force, $w_j(r) \equiv -k_B T \ln g_j(r) = q_j\psi(r) + Jj(r)$, contains the contributions from the electrostatic and hard-sphere correlations, between the central nanoparticle and the other species in the fluid. This implies that the mean force is proportional to electrostatic and entropic components, i.e.,

$$F_{wj} = F_{ej} + F_{sj} \tag{19}$$

with $F_{wj} = -d(w_j(r))/dr$, $F_{ej} = -q_j\ d(\psi(r))/dr$, and $F_{sj} = -d(J_j(r))/dr$, respectively. Although the mean force is equal to the sum of the entropic and electrostatic force components, these two components are not independent of each other, since both components (electrostatic and entropic) are dependent functionals of the radial distribution function, $g_j(r)$, implying that charge an size correlations are, in general, coupled.

RESULTS

For the particular case in which the external field (the central nanoparticle) of species γ becomes equal to just another macroion particle of species M, i.e., $\gamma = M$, eqs 11 and 18, for an inhomogeneous fluid, become the HNC/MSA integral equations for an *homogeneous* colloidal dispersion. Here we solve these equations, for the particular case in which the added electrolyte is a 1:1 symmetric salt. We will denote the cations and anions species as $i = +$ and $i = -$, respectively. The counterions ($i = c$), will be taken as equal either to cations or anions, depending of the sign of macroions, such that the charge of the counterions neutralize the total charge on macroions, i.e., $z_c\rho_c = -z_M\rho_M$. Thus, we can have either more cations than anions or vice versa. With this simplification we have reduced our four-species inhomogeneous system to an *homogeneous* fluid of three species ($i = M, +, -$).

We define the induced charge density profile, $\sigma(r)$, around the central macroion, as

$$\sigma(r) \equiv \sigma_M \frac{R_M^2}{r^2} + \frac{1}{r^2} \int_{R_M}^{r} \rho_{el}(y) y^2\, dy \tag{20}$$

where σ_M is the given charge density on the macroions, such that

$$\sigma_M = -\frac{1}{R_M^2} \int_{R_M}^{\infty} \rho_{el}(y) y^2\, dy \tag{21}$$

by the electroneutrality condition, and, thus, eq 20 becomes

$$\sigma(r) = -\frac{1}{r^2} \int_r^{\infty} \rho_{el}(y) y^2\, dy \tag{22}$$

As can be seen from eq 21, $\sigma(r)$, as defined in eq 22, is the negative of the charge induced in the fluid by the central macroion. However, here we will refer to $\sigma(r)$ as the induced charge density profile. In eq 20, the first term on the right-hand side is the central macroion contribution to the charge density

dx.doi.org/10.1021/jp403313k | J. Phys. Chem. B 2013, 117, 11812−11829

profile, and the second term is the induced charge, per unit area, in a spherical shell defined between the surface of the central colloidal particle and a radius r. In eq 22, the right-hand side term is the induced charge, per unit area, from infinity, to a radius r, from the central macroion particle.

$\rho_{el}(y)$, given by eq 14, is a general expression, and can be directly used in eqs 13, 20, 21 and 22 for the CPM, where the colloidal charge is located at the center of the particles. *However, if the charge is homogeneously smeared over the particles surfaces(MCPM), the local charge density profile is, of course, different for this model, and* $\rho_{el}(y)$ *in eq* 14 *needs to be properly rewritten, to explicitly refer to the charge distribution on the colloidal particles.*

In general, from eq 14, $\rho_{el}(y)$ can be expressed as

$$\rho_{el}(y) = \rho_{el}^{\text{ions}}(y) + \rho_{el}^{M}(y) \tag{23}$$

where

$$\rho_{el}^{\text{ions}}(y) = \sum_{j=+,-} q_j \rho_j g_j(y) \tag{24}$$

is the contribution to the charge concentration profile due *only* to the electrolyte, which is the same for the CPM and MCPM, and $\rho_{el}^{M}(y)$ is the contribution to the charge concentration profile due *only* to the macroion's charge, which is *different* for each of these two models. For CPM, $\rho_{el}^{M}(y)$ is given by

$$\rho_{el}^{M}(y) = q_M \rho_M g_M(y) \tag{25}$$

where $g_M(y)$, calculated with eq 18 (for $j = M$), is, of course, the reduced probability of finding the center of a colloidal particle, at a distance y from the central particle. Therefore, $g_M(y)$ is also the probability of finding a charge q_M in y. For MCPM, the charge concentration profile is also given by eq 23, with $\rho_{el}^{\text{ions}}(y)$ given by eq 24, but to have the corresponding expression for $\rho_{el}^{M}(y)$, we need to calculate the charge distribution, *in the fluid*, due to the charge smeared on the surface of the colloidal particles, i.e., we need the distribution function, $g_M^s(y)$, of infinitely thin, spherical shells, centered around each macroion in the fluid, from which the radial distribution function, $g_M(y)$, around the central macroion, is also obtained with eq 18 (for $j = M$).

In Figure 3 we show two spheres: one centered in the coordinate system (particle 1), and another above, on the z-axis

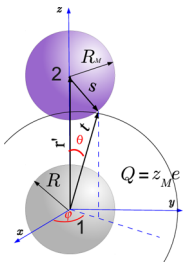

Figure 3. Geometrical sketch, to calculate the homogeneously distributed charge on a MCPM colloidal particle, located at a distance r', from the central particle.

(particle 2). The two particles have a radius, R_M, and, if the charge $Q = ez_M$ is homogeneously smeared on their surfaces, the charge density distribution function, in spherical coordinates, i.e., $dV = t^2 \sin(\theta)\, d\theta\, d\phi\, dt$, on particle 1, is given by

$$\rho(\mathbf{t}) = \frac{Q}{4\pi R_M^2}\delta(t - R_M) \tag{26}$$

In terms of the vectors $\vec{s}$, $\vec{r}'$ and $\vec{t}$ (see Figure 3), such that $\sin\theta\, d\theta = s\, ds/r't$, and hence $dV = ts\, dt\, ds\, d\phi/r'$, the charge density on the sphere in the z-axis (particle 2) is

$$\rho_M(\vec{r}' + \vec{R}_M) = \frac{z_M e}{4\pi R_M^2}\delta(s - R_M) \tag{27}$$

Hence, the total charge on particle 2 is

$$Q = \frac{z_M e}{4\pi R_M^2 r'} \int_{r'-R_M}^{r'+R_M} t\, dt \int_{r'-t}^{r'+t} \delta(s - R_M) s\, ds \int_0^{2\pi} d\phi$$
$$= \frac{z_M e}{2R_M r'}\left[\frac{t^2}{2}\right]_{r'-R_M}^{r'+R_M} = z_M e \tag{28}$$

as expected.

Thus, with the calculated radial distribution function for colloids, $g_M(r')$, from eq 18, it is possible to obtain the contribution of the colloidal particles, in the MCPM, to the charge distribution profile, $q_M \rho_M g_M^s(r')$. Here we emphasize that $g_M(r')$ gives the distribution of the colloidal particles, of species M, with respect the central macroion, and $g_M^s(r')$ gives the distribution of spherical shells, with respect to the central colloidal particle. This spherical shells distribution profile in the MCPM can be written in terms of radial distribution function of the macroions as

$$g_M^s(r') = \frac{1}{4\pi R_M^2 r'} \int_{r'-R_M}^{r'+R_M} g_M(t) t\, dt \times \int_{r'-t}^{r'+t} \delta(s - R_M) s\, ds \int_0^{2\pi} d\phi \tag{29}$$

Hence,

$$g_M^s(r') = \frac{1}{2R_M r'} \int_{r'-R_M}^{r'+R_M} g_M(t) t\, dt \tag{30}$$

To evaluate this integral, we choose two intervals: $r' \in [R_M, 3R_M]$ and $r' > 3R_M$. For $r' \in [R_M, 3R_M]$, we have

$$g_M^s(r') = \frac{1}{2R_M r'} \int_{2R_M}^{r'+R_M} g_M(t) t\, dt \tag{31}$$

and for $r' > 3R_M$

$$g_M^s(r') = \frac{1}{2R_M r'} \int_{r'-R_M}^{r'+R_M} g_M(t) t\, dt \tag{32}$$

With $g_M^s(r')$, calculated with eq 30, and $g_M(r)$, obtained from 18, it is now possible to calculate the colloid particles charge distribution contribution, to the total charge concentration profile, $\rho_{el}(y)$, given by eq 23, i.e.,

$$\rho_{el}^{M}(y) = q_M \rho_M g_M^s(y) \tag{33}$$

which we emphasize is the contribution to the charge concentration profile due *only* to the charge smeared on the macroions' surfaces. With $\rho_{el}(y)$, as obtained above for the CPM and MCP, we can calculate the induced charge density profile, $\sigma(r)$, and the potential of mean force, $\psi(r)$, for these two models.

Summarizing, although for the CPM and MCPM the radial distribution functions, $g_i(r)$, for $i = M, +, -$, obtained with eqs 12 and 18, are all the same for both models, since, according

dx.doi.org/10.1021/jp403313k | J. Phys. Chem. B 2013, 117, 11812−11829

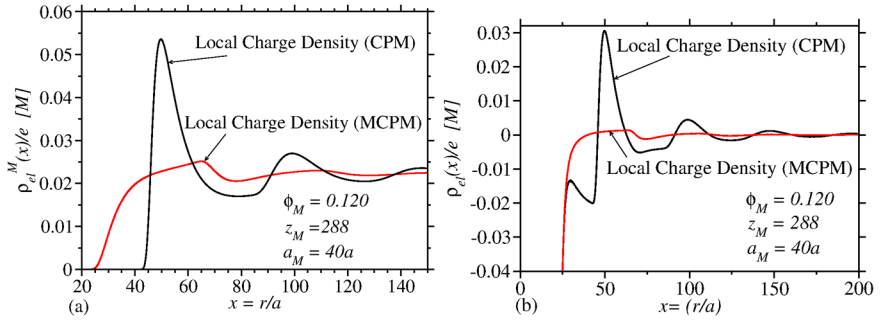

Figure 4. (a) Charge concentration profile, associated only with the macroions, as a function of the distance to the central colloidal particle, for the CPM, $z_M\rho_M g_M(x)$, (solid black line), and MCPM, $z_M\rho_M g_M^s(x)$, (solid red line). The colloid−colloid radial distribution functions, $g_M(r)$, are the same for the two models. The profiles are for a colloid diameter $a_M = 40a$, valence $z_M = 288$, equivalent to a charge surface density $\sigma_M(r) = 0.05C/m^2$, and a bulk density concentration of $\rho_M = 7.7450 \times 10^{-5}$ M, equivalent to a volume fraction $\phi_M = 0.120$. Their counterions (negative ions) satisfy the total electroneutrality condition, and are the same as the anions of the 1:1 added salt, of $\rho_s = 0.1$ M. (b) Total charge concentration profile, i.e., including the little ions.

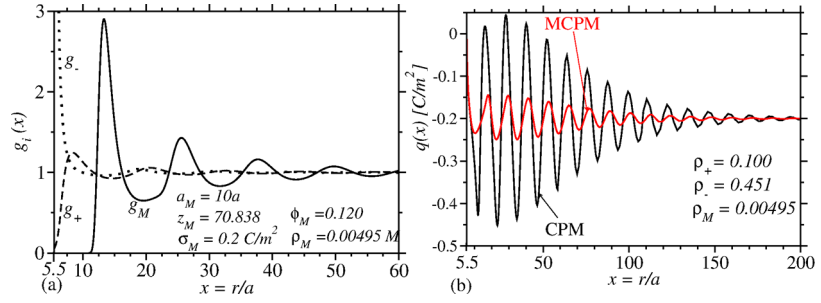

Figure 5. (a) Radial distribution functions for co-ions, g_+, counterions, g_-, and macroions, g_M, around the central macroion. The inset shows the local charge distribution, associated to the macroions profile, for both models, in moles of charge per liter. (b) Accumulated charge density profile $q(x)$ as a function of the distance to the central macroion for both models and for the same parameters of (a).

with Gauss' law, the unscreened interaction potential, given by eq 8, is the same for both models, the charge concentration profile, $\rho_{el}(y)$, is, of course, different, since this quantity, as well as the mean electrostatic potential and the induced charge density, depends on the charge distribution, which is different for these two models.

In Figure 4a we show an example of the charge concentration profile, associated *only* to the macroions, as a function of the distance to the central particle, for the CPM, $\rho_{el}^M(y)/e \equiv Z_M\rho_M g_M(y)$, and the MCPM, $\rho_{el}^M(y)/e \equiv Z_M\rho_M g_M^s(y)$. As one could expect, the charge profile for the MCPM is much more smooth, as a function to the distance to the central colloidal particle. The peak in the CPM profile is due to the adsorption of colloidal particles, to the central colloidal particle, at around $r = 50a$. However, notice that there is some qualitative correspondence between the two models charge distribution profiles, in the location of their maxima and minima. In Figure 4b we show the total charge concentration profile, i.e., $\rho_{el}(y)/e \equiv (\rho_{el}^M(y) + \rho_{el}^{ions}(y))/e$ (see eqs 23, 24, and 25). The CPM total charge profile, has additional structure, due to the little ions, than that associated only to the macroions. There is a wiggle for $x < 40$, showing that little counterions are around two positive macroions at a distance $x \approx 50$. This wiggle is not present in Figure 4a, since the CPM-$g_M(x)$ is equal to zero, for $x < 40$. The CPM-maxima, however, remain in the same position as in Figure 4a. The MCPM maintains the same qualitative behavior, as in Figure 4a, and quickly goes to zero for increasing values of x. However, for both models, the total charge profile for $x = 20.5$ is high, i.e., for the macroion−counterion contact distance, $\rho_{el}(y)/e = -0.7956M$ for CPM, and $\rho_{el}(y)/e = -0.7914M$ for MCPM (not shown), due, of course, to the adsorption of the little counterions to the positively charged central macroion.

Figure 4b clearly shows that different charge distribution on the macroions produce different charge concentration profiles in the fluid, thereby implying different fluid behaviors, and sometimes, as it is shown in this paper, very different behaviors of relevant quantities. The use of such a simple model as the Primitive Model for colloidal dispersions, as in this paper, also shows that interesting complex systems, such as hairy colloidal particles, micelles, vesicles, and/or dendrimers, can be studied with well-established formal liquid theories, such as integral equations, density functional, and/or Modified Poisson−Boltzmann, and realistically solved.

$\psi(r)$ and $\sigma(r)$ Profiles for the CPM and MCPM. In Figure 5a we show the radial distribution functions for a macroion dispersion, in a 1:1 electrolyte. The labels M, +, and − correspond to macroions, co-ions, and counterions, respectively. The counterions valence is equal to that of the anions ($z_- = z_c = -1$), henceforth we also use a minus sign to denote the counterions. The co-ions are positive ions ($z_+ = 1$). In all cases, the co-ions concentration is $\rho_+ = 0.1$ M. For the anions ($z_- = -1$) $\rho_- \geq \rho_+ = 0.1$ M, i.e., the sum of the salt anions concentration, plus the macroions' concentration. Hence, $\rho_- = 0.1 + z_M\rho_M$, to satisfy the colloidal dispersion electroneutrality condition. The diameter of the little ions is $a_+ = a_- = a = 4.25$ Å. The macroions have $\rho_M = 0.00495$ M, equivalent to a volume fraction $\phi_M = 0.12$, defined as $\phi_M = \pi\rho_M a^3/6$. The macroion valence is $z_M = 70.838$, equivalent to a surface charge density $\sigma_M = 0.2\ C/m^2$, given that $a_M = 2R_M = 10a$. As pointed

dx.doi.org/10.1021/jp403313k | J. Phys. Chem. B 2013, 117, 11812−11829

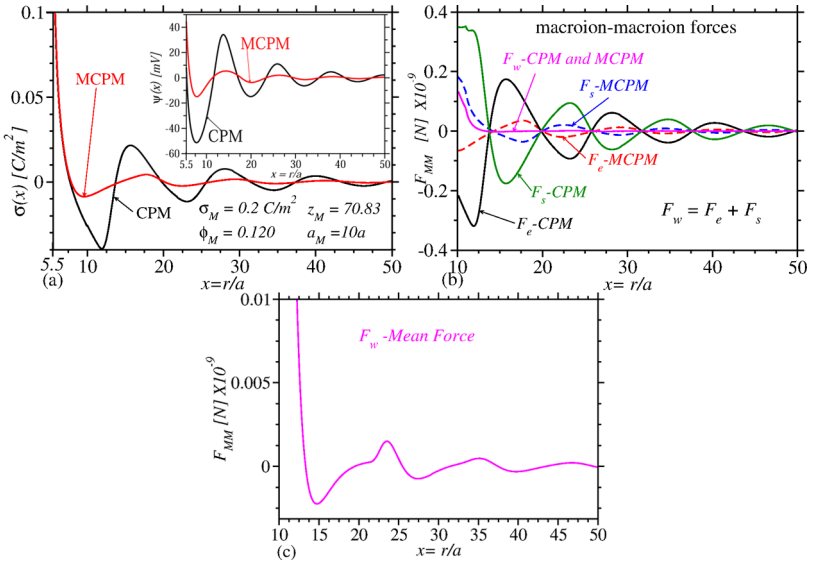

Figure 6. (a) Induced charge density profiles, $\sigma(x)$, with their respective mean electrostatic potential, $\psi(x)$, for both models, shown in the inset. (b) Electrostatic forces, entropic forces and mean force for both models. All parameters employed are the same as those in Figure 5. (c) Mean force for both models.

out above, $g_+(x)$, $g_-(x)$, and $g_M(x)$, are the same calculated with both models, i.e., for the CPM and the MCPM.

In Figure 5a, near the central macroion, there is a high concentration of anions (dotted line) and low for cations (dashed line), while there is a macroion−macroion repulsion (solid-line) at the contact, followed by a high attractive peak (first maximum), and then damping oscillations. These HNC/MSA results have been shown in the past to be in good agreement with molecular dynamics results.[63] With the radial distribution functions it is possible to compute the $\sigma(r)$ and $\psi(r)$ profiles. The charge concentration profiles, associated only to the macroions, in the CPM, $z_M\rho_M g_M(x)$, and MCPM, $z_M\rho_M g_M^s(x)$, as a function of the distance to the central colloid particle, are given in the inset of Figure 5a. The charge distribution for the MCPM initiates closer to the central colloid particle, than that for the CPM. The maxima and minima in the CPM are much larger than those for the MCPM. These differences are, of course, due to the different distributions of the colloidal charge in the two models.

Another interesting quantity is the adsorbed charge, $q(r)$, defined as the accumulated charge, from the contact position, $r = R_M + a/2$, up to some arbitrary position, r, in the fluid, divided by the area of the central macroion, and is given by

$$q(r) = \frac{1}{R_M^2}\int_{R_M+a/2}^{r} \rho_{el}(y)y^2\,\mathrm{d}y \tag{34}$$

The $q(x{\equiv}r/a)$ profile shown in Figure 5b converges to $\lim_{r\to\infty} q(x) = -0.2\ C/m^2$, i.e., the total induced charge, which is of equal magnitude and of opposite sign to the charge on the central macroion, in agreement with the electroneutrality condition. $q(x)$ oscillates around -0.2 C/m^2, and is in general lower than 0. However, $q(r) > 0$ implies that the total charge inside of a spherical surface of radius r, around the central macroion is larger than that of the central colloidal particle, i.e., $q(r) > 4\pi R_M^2\sigma M$. There is a long-range oscillatory behavior of $q(x)$. In both models, there is a fast screening of the central macroion, i.e., at $x \approx [7.7,7.9]$, $q(x) \approx -0.2$ C/m^2 (the charge of the central macroion), implying that the screening is mainly due to the charge of counterions (anions) attached as a "cloud" to the surface of the adsorbed macroions. The high coincidence between the $q(x)$ profiles for both models, in the interval ($x \in [5.5,7.9]$) is because, at this short distance, there is not a significant effect due to the charge distribution on the colloidal particles. For larger values of x, however, there is an important disagreement. For CPM there is an increasing negative value of $q(x)$, up to $q(x) \approx -0.45$ C/m^2, which implies almost a double overcompensation of the charge on the colloidal particle (charge reversal). This charge reversal is well above that observed for the MCPM profile, of $q(x) \approx -0.23$ C/m^2. The value of $q(x) \approx -0.23$ C/m^2 for MCPM indicates a very low charge reversal, since its difference with respect to the screening value is just -0.03 C/m^2, only about 15%, which contrasts with that of the CPM, -0.25 C/m^2. $q(x)$ shows the important effect of the charge distribution on the colloidal particle on the mean electric field: $q(x)$ is considerably lower in MCPM than its counterpart in the CPM (see inset in Figure 5a). This behavior is general, i.e, it was observed for different conditions of volume fraction, ϕ_M, different sizes of colloids, a_M, and different surface charge densities, σ_M.

Differences between the two models, can also be observed in the induced charge density profiles, $\sigma(x)$, and mean electrostatic potential profile, $\psi(x)$ (see Figure 6a). Notice that $\sigma(r) = (R_M/r)^2[\sigma_M + q(r)]$. The lower induced charge, due to the macroions adsorption to the central macroion, in the MCPM (see inset in Figure 5a), promotes lower values of the mean electrostatic potential profiles, with respect to that of the CPM, and has a direct impact on the electrostatics forces, since, by Gauss law, $\mathbf{E}(x)$ is proportional to the charge density enclosed by a concentric surface of radius x. Thus, for less charge density, the electrostatic field is lower. On the other hand, since $E_i(x) = -q_i(x)\,\mathrm{d}\psi(x)/\mathrm{d}(x)$, and the slope of the $\psi(r)$ profiles in Figure 6a (inset) is softer for MCPM than that of the CPM, this implies a lower electrostatic field for MCPM. The $F_{MM}(x)$ colloid−colloid forces are shown in Figure 6b and Figure 6c. We show the electrostatic, $F_e(x)$, and entropic, $F_s(x)$, components of the mean force, $F_w(x)$. As expected, the mean force, shown in Figure 6c, results to be the same for both models, i.e., $F_w(x) = -\mathrm{d}(-\ln(g_M(x))/k_BT)/\mathrm{d}x$, where k_B is the

dx.doi.org/10.1021/jp403313k | J. Phys. Chem. B 2013, 117, 11812−11829

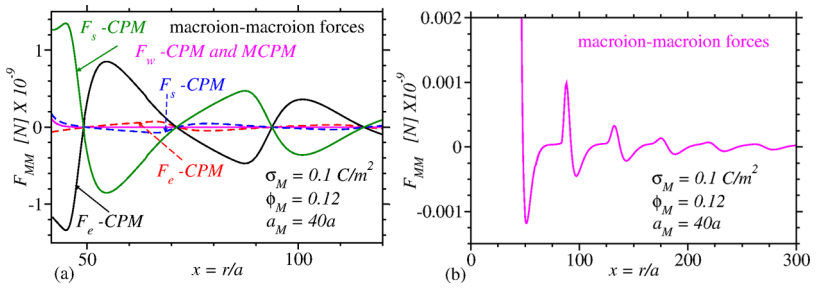

Figure 7. (a) Electrostatic forces, entropic forces, and mean force for both models for a macroions dispersion of $a_M = 40a$. (b) Mean force for both models, at a larger scale. All other parameters are the same as in Figure 5.

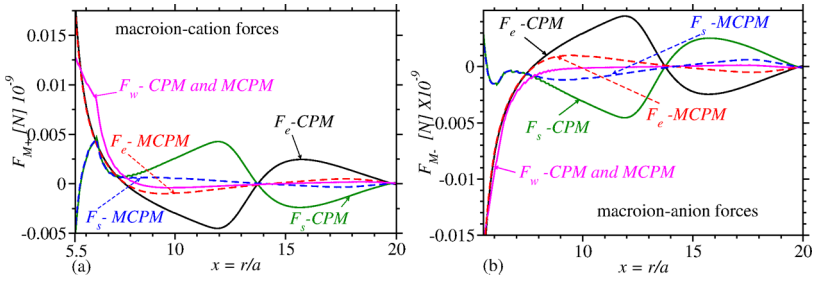

Figure 8. (a) Macroion−cation and (b) macroion−anion electrostatic, entropic, and mean forces, for both models. All parameters employed are the same as those in Figure 5. The mean force is also shown (fuchsia).

Boltzmann constant, and T the absolute temperature. Here we have dropped the species subindexes for notation simplicity. The fact that the radial distribution functions, $g_M(x)$, $g_+(x)$, $g_-(x)$, and $g_c(x)$, are all the same for both CPM and MCPM, but the electrostatic and entropic forces are different, implies that *there is not a unique combination of the electrostatic and entropic components of the mean force, such that* $F_w(x) = F_e(x) + F_s(x)$. To the best of our knowledge, this finding has not been reported in the past.

The mean force components, for both models, have approximately the same qualitative behavior, although they have important quantitative differences (see Figure 6b). At short colloid−colloid distance ($x \lesssim 13.66$ Å), although the mean force is repulsive, the electrostatic force between macroions, for the CPM is *attractive*, whereas the entropic force is *repulsive*. The same behavior of these forces is observed in the case of MCPM, although with less intensity. More important, however, is the fact that *the mean force components, and the mean force itself, show a long-range oscillatory (attractive-repulsive) behavior*. We stress the fact that our calculations are for a finite concentration colloidal dispersion in a 1:1 electrolyte, with an ionic size of $a = 4.25$ Å. This is an interesting result. In the past, for colloidal dispersions, at infinite dilution, i.e., for two like-charged planar,[5,11,12,15,18,24,80] spherical,[26,81] and cylindrical[27] colloidal particles, immersed in a 1:1 primitive model electrolyte, with an ionic size of $a = 4.25$ Å, their electrostatic, entropic, and total mean forces were found to be everywhere repulsive. Although, for two cylinders immersed also into a 1:1 electrolyte, but with a larger hydrated ionic size[70] $a = 8$ Å, an attractive entropic and total mean force was found to be oscillatory (attractive-repulsive),[27] although of short-range ($r \gtrsim 3a$), whereas the electrostatic component is everywhere repulsive. This short-range attraction for larger ionic sizes emphasizes the entropy contribution to the mean force. Also for this system but in a 2:2 electrolyte, the electrical force is attractive, whereas the entropic force is mainly repulsive, and hence an attractive region of the total mean force, is found. This attraction, however, is of very short-range, i.e., $r \lesssim 3a$ in cylindrical geometry,[27] and $r \lesssim 1.8a$ for spherical geometry.[81]

At short colloid−colloid distances, although not only, F_{eM} is very attractive. This short-range, attractive, electrical force is due to the high local concentration of counterions (see Figure 5a), whereas F_{sM} is repulsive because of an enhanced excluded volume in between the two colloids, due to the counterion-counterion repulsive correlation. This effect is qualitatively lower in the MCPM, where the local accumulated charge distribution (see Figure 5b) shows less total charge from counterions respect to that of the CPM, which is equivalent to less repulsive counterion-counterion electric force, hence, less excluded volume, which is seen in their corresponding macroion-macroion force profiles (see Figure 6b, Figure 7a, and Figure 7b).

For a constant $\phi_M = 0.120$, this general qualitative behavior was also found for larger values of a_M or σ_M. For a constant σ_M, but increasing a_M, their respective $\psi(x)$, $q(x)$, $\sigma(x)$ and forces profiles are magnified, due to the larger values of z_M, which increases as a_M increases, i.e., $z_M \propto \sigma_M a_M^2$. Also the difference between the MCPM and CPM results increases, with increasing values of σ_M, since with larger values of z_M, the macroion-macroion correlation increases, and this is more notorious in CPM. An electrostatic attraction between two like-charged colloids, in a finite concentration colloidal dispersion, based on a counterions attraction mechanism, through semiphenological theories, has been proposed and studied in the past to explain long-range colloids ordering and phase transitions.[47,82−85]

The attraction between like-charged particles, based on purely electrostatic mechanisms, has been debated.[86−88] Here we have shown, through a well-established integral equations theory, that, indeed, not only is the electrostatic component of the like-charged colloid−colloid mean force attractive at short-range, but it also has a long-range oscillatory behavior. The range of this electrostatic force component depends on the macroion sizes, i.e., the long-range attraction increases with

increasing macroions size: compare Figure 6b,c, for a macroion size of $a_M = 10a$, with Figure 7a,b, for a macroion size of $a_M = 40a$. Hence a long-range electrostatic attraction is demonstrated. However, as pointed out above, in the macroion infinite dilution case, all forces are repulsive for the 1:1 electrolyte case,[81] showing the importance of the volume fraction, i.e., the overall entropy contribution to the colloidal dispersion structure. It should also be pointed out that, although one can calculate the electrostatic and entropic components of the mean force, they are not independent, since the electrostatic and entropy components of the potential of mean force are tangled through eqs 18 (see also eq 19). The mean force becomes of longer range, as the macroions diameter increases (see Figure 6c and Figure 7b). In general, everything else being the same, higher volume fraction implies longer oscillatory macroion−macroion correlation. This long-range correlation for large particles becomes very long-range, and could be responsible of the voids and phase transitions experimentally reported.[47,82−84] In Figure 9 we show the macroion−macroion

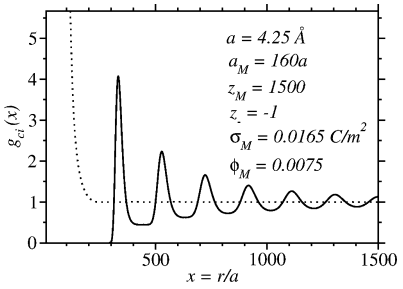

Figure 9. Macroion−macroion (solid line) and macroion−counterion (dotted line) radial distribution functions for a macroions dispersion of $a_M = 160a$, in the absence of salt.

and macroion−anion radial distribution functions for a macroion dispersion, in the absence of salt. The macroion diameter is $a_M = 160a$, with $\rho_M = 7.5635 \times 10^{-8} M$ (ϕ_M = 0.0075). The counterion concentration is $\rho_M = 1.135 \times 10^{-4} M$, while their diameter is $a = 4.25$ Å. Here we wish to emphasize the much larger macroion−macroion correlation, as compared to the cases of $a_M = 10a$ (see Figure 5a), and $a_M = 40a$ (see Figure 7). In fact, the macroion correlation goes well beyond 10 000 Å (not shown), i.e., more than the equivalent of 3300 water molecules apart, or more than 15 macroion's diameters apart.

In Figure 8, we show the mean force components for the case of the macroion−counterion (anion) and macroion−co-ion (cation) mean force. Here the electric component of the mean force has the expected behavior, at short distance, i.e., it is repulsive, in the case of attractive in the macroion−anion case, and repulsive in the macroion−cation case. The entropic component is repulsive (attractive), at very short macroion−anion (macroion−cation) distances, to rapidly become attractive (repulsive), up to a distance, $r \gtrsim 13.5a$, to become oscillatory for larger distances. Their corresponding reduced distribution functions, $g_i(r)$, are shown in Figure 5a. At very short distances (up to $r \cong 7.5a$) the electrostatic and entropic components, for both CPM and MCPM, coincide, since at these very short distances, the effect of the charge distribution on the colloidal particle is not seen by the little ions, i.e., the next macroion away from the central macroion is at $r \gtrsim 11a$ (see Figure 5a).

In Figure 10, we show only the $\psi(x)$ profiles, for different σ_M, since all other profiles ($q(x)$, $\sigma(x)$ and forces) have a similar behavior, in both models. In Figure 10a we show the MCPM $\psi(x)$ profiles for, $a_M = 10a$ and $\phi_M = 0.120$. We observe that as σ_M increases, the amplitude of the oscillations in the $\psi(x)$ profiles increases significantly, as one could expect for higher electrical fields. Notice the shift of the whole curves to the left, showing greater colloid−colloid correlation. This general behavior also is found for CPM (see Figure 10b). A comparison with the MCPM results of Figure 10a shows very important quantitative differences, but the same qualitative behavior. In Figure 10c, we compare MCPM with the CPM, for $a_M = 40a$.

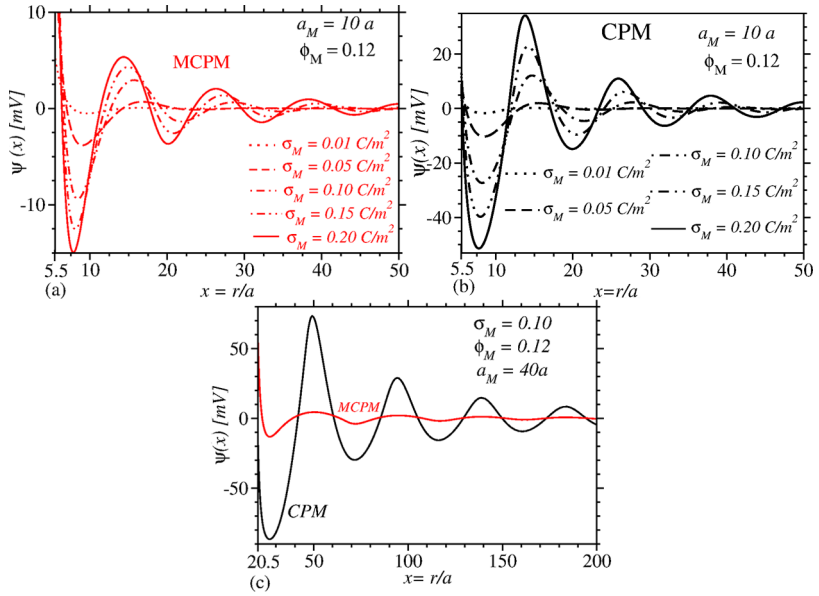

Figure 10. (a) Mean electrostatic profiles, $\psi(x)$, for MCPM (red lines) for different surface charge density, σ_M, values, such that $a_M = 10a$ and $\phi_M = 0.12$. (b) Mean electrostatic potential profiles, $\psi(x)$, for CPM. (c) Comparison of the $\psi(x)$ profiles between the MCPM (red lines) and CPM (black lines), for a macroions solution with $a_M = 40a$ and $\phi_M = 0.12$, for different σ_M values.

dx.doi.org/10.1021/jp403313k | J. Phys. Chem. B 2013, 117, 11812−11829

Here is seen the long-range electrostatic correlation in both models of colloidal dispersions.

The ζ-Potential. An important quantity, measured to characterize the charge of colloidal particles, is the electrophoretic mobility. In electrophoresis experiments, an external electrostatic field is applied to a diluted solution of charged colloidal particles, and their mobility is measured, defined as $\mu = |\mathbf{U}|/|\mathbf{E}|$, where $\mathbf{U}$ and $\mathbf{E}$ are the observed velocity and applied electrostatic field respectively. μ can be correlated to the ζ-potential, i.e., the mean electrostatic potential measured on the slipping surface, which refers to the surface that separates a colloidal particle moving together with the near part of its electrical double layer, with respect to the rest of the fluid.[89] To calculate the ζ-potential, a statistical mechanics theory is needed.[34,90−92] For large colloidal particles, a first simple theory, for the mobility of colloidal particles at *infinite dilution* is the Smoluchowsky theory.[89] In this theory, $\mu = \varepsilon\zeta/\eta$, such that ε is the dielectric constant, ζ is the ζ-potential, and η is the viscosity. Despite its simplicity, the Smoluchowsky approach could give some indication of the mobility and the nature of the colloidal charge. In this work we assume the slipping surface located at $x = (R_M + a/2)$, and, hence, the ζ-potential = $\psi(R_M + a/2)$.

In previous papers,[62,63] for the CPM, it was found a high inversion of ζ-potential, for increasing colloidal surface charge density, σ_M, and/or increasing colloidal diameter, a_M (see Figure 11). An inversion of the ζ-potential implies a reverse electrophoretic mobility. A reverse electrophoretic mobility has been long theoretically predicted,[23,32,34−37] reported by computer simulations,[39,44,93,94] and experimentally measured.[33,42,46] This inversion of the ζ-potential is due to a high overcompensation of charge on the central colloidal particle, i.e., a magnified charge reversal due to mainly entropy effects,[23,34,44,55,56,95] and not only by energy, as in Wigner-crystal, cero temperature, models.[35,36,40,44,68] The results here presented for the CPM confirm the role of entropy in the charge reversal, and hence a reverse electrophoretic mobility, if one takes Smoluchowsky theory as a first approximation. Notice that larger a_M implies larger z_M and more counterions coupling. For $\phi_M \to 0$, i.e., infinite dilution, important quantitative, and even opposite qualitative behavior of the ζ-potential with a_M is found, i.e., for the infinite dilution case, there is no maximum, as a function of σ_M, and we find an increasing ζ-potential, for increasing macroion size, a_M, hence, there is no inversion of the ζ-potential. This implies that the overcompensation decreases, i.e., the effect of colloid's surface charge is more important on the ζ-potential, in finite concentration colloidal dispersions, i.e., notice the fast convergence of the ζ-potential to its limiting value, at $a_M \to \infty$, for $a_M = 40a$.

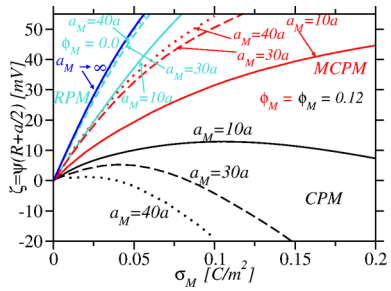

Figure 11. ζ-potential as a function of σ_M, for MCPM and CPM; also shown is the limit case where $\phi_M \to 0$, known as restrictive primitive model (RPM). The MCPM and CPM are respectively represented by red and black lines, for three different diameters, i.e., $a_M = 10a$ (solid lines), $a_M = 30a$ (dashed lines) and $a_M = 40a$ (dotted lines). The RPM is represented by turquoise lines, for $a_M = 10a$, $a_M = 30a$ and $a_M = 40a$, following a similar notation, and only the special case when $a_M \to 0$ is denoted as a solid blue line.

For MCPM, at finite concentration, we find a similar qualitative behavior to that of the macroions at infinite dilution case, i.e., the ζ-potential increases with increasing a_M, and there is no maximum, and not an inversion of the ζ-potential. Thus, the effect of distribution of charge on the particle's surface has a significant effect on the value of ζ-potential, and, therefore, also on the electrophoretic mobility. Notice, however, the very important quantitative differences between the MCPM ζ-potential with that for the infinite dilution case. Interesting studies of the electrophoretic mobility, for colloidal dispersions at finite concentration, have been performed by Palberg et al.[43,96−99] Their results are presented as a function of the volume fraction. In particular, they find that the mobility has a maximum, i.e., at very low volume fractions, the mobility increases,[96] but decreases at higher volume fraction.[43] A comparison of the mobility, obtained with our theory, with Palberg's simulation results will be presented in a forthcoming work.

CONCLUSIONS

It has been shown that, in spite of the fact that all radial distribution functions in both the CPM and MCPM are exactly the same, and, hence also both models have the same potentials of mean force, their mean electrostatic potentials and induced charge profile, have very important quantitative differences. Basically, the MCPM profiles are smoother than those from the CPM. However, a key quantity such as the ζ-potential has an opposite behavior, in the two models. While the colloid−colloid potential of mean force is the same in both models, and hence the mean force is also the same, their electrostatic and entropic components are different. Therefore, as a general result, we find that the stability conditions of a colloidal dispersion do not depend on the particular distribution of the charge on the colloidal particles, but their electrical characterization does. Hence, the electrophoresis studies depend not only on the amount of charge in the colloidal particle, but also on its distribution. If the distribution of charge is not known, the electrophoresis studies might give unreliable results. We find that the electrostatic and entropic components of the mean force are oscillatory, and of long-range, giving support, on the one hand, to a long-range electrostatic attraction mechanism between like-charged colloids, debated in the literature as responsible of voids and phase transitions, experimentally found in charged colloidal dispersions,[47,82,83] and, on the other hand, to the so-called volume term theory,[85−88] in particular due to the long-range entropic component of the force. In our theory, the electrostatic and entropic components of the mean force are not independent of each other. Hence, the oscillatory behavior of the colloid−colloid radial distribution function obtained in our theory, indicates a long-range like-charged colloid−colloid correlation of electrostatic and entropic origin.

dx.doi.org/10.1021/jp403313k | J. Phys. Chem. B 2013, 117, 11812−11829

APPENDIX A: THE MEAN SPHERICAL APPROXIMATION

To solve our inhomogeneous fluids integral equations (eq 7), we need the bulk direct correlation functions, $c_{ij}(s)$, obtained from eq 6. In this study we use the analytical MSA expressions for $c_{ij}(s)$, derived in the past by Hiroike and Blum, i.e.,[73−75]

$$sc_{lj}(s) = sc_{lj}^{sr}(s) + sc_{lj}^{hs}(s) - \frac{\beta q_l q_j}{\varepsilon} \tag{35}$$

with $c_{lj}^{sr}(s) = (e^2\beta/\varepsilon)d_{ij}(s)$, where

$$sd_{lj}(s) = \begin{cases} s\zeta_{lj} + z_l z_j & \text{for } 0 \le s \le \lambda_{lj} \\ o_{lj} + z_l z_j - s\gamma_{lj} + s^2\eta_{lj} + s^4\varsigma_{lj} & \text{for } \lambda_{lj} \le s \le a_{lj} \\ 0 & \text{for } s > a_{lj} \\ \text{with } i, j = 1, ..., 4, & \end{cases} \tag{36}$$

with $\lambda_{lj} \equiv |a_l - a_j|/2$, $a_{lj} \equiv (a_l + a_j)/2$, and

$$\zeta_{lj} = -2\left[-z_l n_j + x_l s_l - \frac{a_l}{3}s_l^2\right] \tag{37}$$

$$o_{lj} = (a_l - a_j)\left[\frac{x_l + x_j}{4}(s_l - s_j) - \frac{a_l - a_j}{16}[(s_l + s_j)^2 - 4n_l n_j]\right] \tag{38}$$

$$\gamma_{lj} = (x_l - x_j)(n_l - n_j) + (x_l^2 + x_j^2)\Gamma + (a_l + a_j)n_l n_j - \frac{1}{3}(a_l s_l^2 + a_j s_j^2) \tag{39}$$

$$\eta_{lj} = \frac{x_l}{a_l}s_l + \frac{x_j}{a_j}s_j + n_l n_j - \frac{1}{2}[s_l^2 + s_j^2] \tag{40}$$

$$\varsigma_{lj} = \frac{1}{6}\left[\left(\frac{s_l}{a_l}\right)^2 + \left(\frac{s_j}{a_j}\right)^2\right] \tag{41}$$

where $s_l = n_l + \Gamma x_l$ and $x_l \equiv z_l + n_l a_l$. z_l and a_l are the valence and diameter, respectively, of species l. The Γ and n_l functions are obtained numerically from the following algebraic equations:

$$\Gamma^2 = \frac{\pi e^2\beta}{\varepsilon}\sum_{l=1}^{4}\rho_l(z_l + n_l a_l)^2 \tag{42}$$

and

$$-x_l\Gamma = n_l + ca_l\sum_{l=1}^{4}\rho_l a_l x_l \tag{43}$$

with $c = (\pi/2)[1-\pi/6\Sigma_{l=1}^{4}\rho_l a_l^3]^{-1}$. ρ_l is the number density, and a_l is the diameter of the species l.

The $c_{lj}^{hs}(s)$ function is given by

$$sc_{lj}^{hs}(s) = \begin{cases} su_l & \text{for } 0 \le s \le \lambda_{lj} \\ \chi_{lj}(0) + su_{lj} + s^2\tau_{lj} + s^4 W & \text{for } \lambda_{lj} \le s \le a_{lj} \\ 0 & \text{for } s > a_{lj} \end{cases} \tag{44}$$

where

$$u_l = -\left[\frac{1}{1-\xi_3} + aa_l + ba_l^2 + \frac{c}{3}a_l^3\right] \tag{45}$$

$$a \equiv \frac{3\xi_2}{(1-\xi_3)^2} \tag{46}$$

$$b \equiv 3\left[\frac{\xi_1}{(1-\xi_3)^2} + \frac{3\xi_2^2}{(1-\xi_3)^3}\right] \tag{47}$$

$$c \equiv 3\left[\frac{\xi_0}{(1-\xi_3)^2} + \frac{6\xi_1\xi_2}{(1-\xi_3)^3} + \frac{9\xi_2^3}{(1-\xi_3)^4}\right] \tag{48}$$

where $\xi_m = \Sigma_{i=1}^{4}\eta_i a_i^m$ and $\eta_i \equiv \pi\rho_i/6$.

Furthermore,

$$\chi_{lj}(0) = (a_l - a_j)^2\left[\frac{a}{8} + \frac{b}{8}(a_l + a_j) + \frac{c}{32}(a_l + a_j)^2\right] \tag{49}$$

$$u_{lj} = -\frac{u_l + u_j}{2} \tag{50}$$

$$\tau_{lj} = -\frac{\tau_l + \tau_j}{2} \tag{51}$$

$$\tau_l = -\left[\frac{a}{2} + ba_l + \frac{ca_l^2}{2}\right] \tag{52}$$

W is given by

$$W \equiv -\frac{1}{2(1-\xi_3)^4}[\xi_0 + 2(3\xi_1\xi_2 - \xi_0\xi_3) + (\xi_0\xi_3^2 - 6\xi_1\xi_2\xi_3 + 9\xi_2^3)] \tag{53}$$

Hence, substituting eq 35 in the convolution integral of eq 7 and the HNC closure, eq 2, in the first right-hand side term of eq 7, we get eq 11. Therefore, the expressions for the functions $L_{lj}(x,y)$ and $K_{lj}(x,y)$ are found to be

$$L_{lj}(r, t) \equiv \frac{1}{r}\int_{|r-t|}^{|r+t|} c_{lj}^{sr}(s)s\, ds \tag{54}$$

and

$$K_{lj}(r, t) \equiv \frac{1}{r}\int_{|r-t|}^{|r+t|} c_{lj}^{hs}(s)s\, ds \tag{55}$$

Such that

dx.doi.org/10.1021/jp403313k | J. Phys. Chem. B 2013, 117, 11812−11829

$$L_{lj}(r,\,t) = \begin{cases} \dfrac{e^2\beta\zeta_{lj}}{\varepsilon}M_2 + \dfrac{\beta q_l q_j}{\varepsilon}M_1 + \\ \dfrac{\beta e^2}{\varepsilon}[(o_{lj} + z_l z_j)J_1 + \\ \gamma_{lj}J_2 + \eta_{lj}J_3 + \varsigma_{lj}J_5] & \text{for } 0 \le |r-t| \le l_{lj} \\ \dfrac{\beta e^2}{\varepsilon}[(o_{lj} + z_l z_j)N_1 + \\ \gamma_{lj}N_2 + \eta_{lj}N_3 + \varsigma_{lj}N_5] & \text{for } l_{lj} \le |r-t| \le a_{lj} \\ 0 & \text{for } |r-t| > a_{lj} \end{cases}$$

$$\text{with } i, j = 1, \ldots, 4 \tag{56}$$

with $M_m \equiv (\lambda_{lj}^m - |r-t|^m)/rm$, $J_m \equiv (a_{lj}^m - \lambda_{lj}^m)/rm$, $N_m \equiv (a_{lj}^m - |r-t|^m)/rm$, and $a_{lj}^m \equiv [(a_l + a_j/2)]^m$, where $\lambda_{lj}^m \equiv [|al - aj|/2]^m$. Also,

$$K_{lj}(r,\,t) = \begin{cases} u_l M_2 + \chi_{l_j}(0)J_1 + \\ u_{lj}J_2 + \tau_{lj}J_3 + WJ_5 & \text{for } 0 \le |r-t| \le l_{lj} \\ \chi_{l_j}(0)N_1 + u_{lj}N_2 + \\ t\tau_{lj}N_3 + WN_5 & \text{for } l_{lj} \le |r-t| \le a_{lj} \\ 0 & \text{for } |r-t| > a_{lj} \end{cases}$$

$$\text{with } i, j = 1, \ldots, 4 \tag{57}$$

With eqs 56 and 57, we can obtain the analytical expression for eq 16, given by

$$A_j(r) = \sum_{l=M,+,-,c} \rho_l \int_0^{a_{\gamma l}} h_{\gamma l}(t)[L_{lj}(r,\,t) + K_{lj}(r,\,t)]t\ \mathrm{d}t \tag{58}$$

Observe that the Kernels $L_{lj}(r,t)$ and $K_{lj}(r,t)$ from eqs 56 and 57 are different from zero only for $|r-t| \le a_{lj}$. Furthermore, the domain of t in the $A_j(r)$ integral is restricted by its upper limit, i.e., $t \in [0,a_{\gamma l}]$. Therefore, the Kernels will be different from zero only for the values of r that fulfill these restrictions. Also notice that in the interval $t \in [0,a_{\gamma l}]$, the total correlation function $h_{\alpha l}(t) = -1$, since $g_{\alpha t}(t) = 0$.

We can write $A_j(r)$ as $A_j(r) = \Sigma_{l=M,+,-,c}A_{lj}(r)$, where

$$A_{lj}(r) \equiv \rho_l \int_0^{a_{\gamma l}} h_{\gamma l}(t)[L_{lj}(r,\,t) + K_{lj}(r,\,t)]t\ \mathrm{d}t \tag{59}$$

Each $A_{lj}(r)$ function depends on the relative values of a_l and a_j, as shown in Figure 12: The variable t runs within the interval $t \in [t_{min},t_{max}]$, where, $t_{min} = a_{\gamma j} - a_{lj}$ and $t_{max} = a_{\gamma l}$, while r runs within the interval $r \in [r_{min},r_{max}]$, being $r_{min} = a_{\gamma j}$ and $r_{max} = a_l + a_{\gamma j}$. Only when $a_l > a_j$ (case a) can t be larger than r, implying, according to eqs 56 and 57, that there are three nontrivial integration intervals for its respective $A_{lj}(r)$ function. Hence:

1. **The $A_{lj}(r)$ function, when $a_l > a_j$.**

We simplify the notation, labeling eqs 56 and 57 as follows:

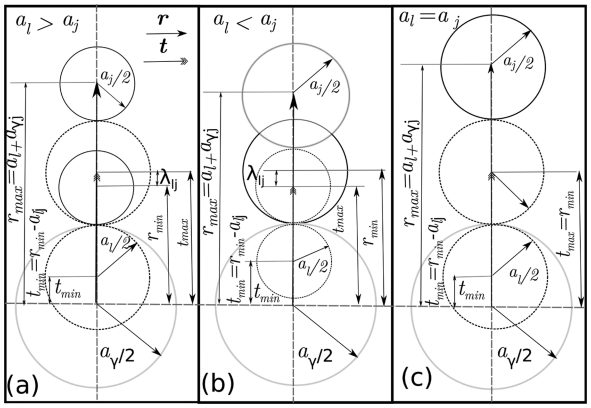

Figure 12. Integration intervals for (a) $a_l > a_j$, (b) $a_l < a_j$, and (c) $a_l = a_j$. The dashed contoured circles represent the $i = l$-species, the solid contoured circles are $i = j$-species, while the bottom light-gray corresponds to the central particle, at infinite dilution (γ-species). Because j-species corresponds to the species located by the **r** position vector, it can not overlap with γ-species, due to the infinite hard sphere potential. Thus $r_{min} = a_{\gamma j} = (a_\gamma + a_j)/2$ and $t_{min} = a_{\gamma j} + a_{lj}$. Also, $r_{max} = a_l + a_{\gamma j}$ and $t_{max} = a_{\gamma l}$. Note that only for the case (a), the t value can be bigger than r, while in the other two cases this can not happen. Remember that $\lambda_{lj} = |a_l - a_j|/2$.

$$L_{lj}(r,\,t) = \begin{cases} L_{lj}^1(r,\,t) & \text{for } 0 \le |r-t| \le l_{lj} \\ L_{lj}^2(r,\,t) & \text{for } l_{lj} \le |r-t| \le a_{lj} \\ 0 & \text{for } |r-t| > a_{lj} \end{cases}$$

$$\text{with } i, j = 1, \ldots, 4 \tag{60}$$

and

$$K_{lj}(r,\,t) = \begin{cases} K_{lj}^1(r,\,t) & \text{for } 0 \le |r-t| \le l_{lj} \\ K_{lj}^2(r,\,t) & \text{for } l_{lj} \le |r-t| \le a_{lj} \\ 0 & \text{for } |r-t| > a_{lj} \end{cases}$$

$$\text{with } i, j = 1, \ldots, 4 \tag{61}$$

Notice that the kernels $L_{ij}^1(r,t)$ and $K_{ij}^1(r,t)$, defined in the interval $0 \le |r-t| \le \lambda_{lj}$, imply, of course, that

$$0 \le |r-t| \le \lambda_{lj} = \begin{cases} 0 \le (r-t) \le \lambda_{lj} & \text{if } r > t \\ 0 \le -(r-t) \le \lambda_{lj} & \text{if } r < t \end{cases} \tag{62}$$

or equivalently,

$$0 \le |r-t| \le \lambda_{lj} = \begin{cases} r \ge t \ge r - \lambda_{lj} & \text{if } t < r \\ r \le t \le r + \lambda_{lj} & \text{if } t > r \end{cases} \tag{63}$$

Analogously, $L_{ij}^2(r,t)$ and $K_{ij}^2(r,t)$, defined in the interval $\lambda_{lj} \le |r-t| \le a_{lj}$, imply that

$$\lambda_{lj} \le |r-t| \le a_{lj} = \begin{cases} r - \lambda_{lj} \ge t \ge r - a_{lj} & \text{if } t < r \\ r + \lambda_{lj} \le t \le r + a_{lj} & \text{if } t > r \end{cases} \tag{64}$$

Since in these equations the t-variable can be lower than r ($t < r$) or larger ($t > r$), is necessary to carefully analyze the intervals of validity, in eqs 63 and 64, according to the case to

dx.doi.org/10.1021/jp403313k | J. Phys. Chem. B 2013, 117, 11812−11829

be treated. In general, $t < r$; however, if $r \in [r_{min} = a_{\gamma j}, a_{\gamma l} = t_{max}]$, where $[a_{\gamma j}, a_{\gamma l}] \subset [r_{min}, r_{max}]$, then t can be lower or larger than r, i.e., $r < t$ or $t > r$, within the integration interval (see Figure 12). Notice that if $r > t_{max}$, necessarily $t < r$, since t will exceeds its maximum value. Hence, it is possible to define the functions $\Lambda_1(r)$, $\Lambda_1^{(a)}(r)$, and $\Lambda_1^{(b)}(r)$, such that $\Lambda_1(r) = \Lambda_1^{(a)}(r) + \Lambda_1^{(b)}(r)$, where:

(i) $\Lambda_1^{(a)}(r)$ is defined only for $t < r$, i.e.,

$$\Lambda_1^{(a)}(r) \equiv \rho_l \int_{r-a_{lj}}^{r-\lambda_{lj}} [-1][K_{lj}^2(r,t) + L_{lj}^2(r,t)]tdt + \rho_l \int_{r-\lambda_{lj}}^{r} [-1][K_{lj}^1(r,t) + L_{lj}^1(r,t)]tdt \quad (65)$$

In eq 63, for $t < r$, the allowable values of t are $r \geq t \geq r - \lambda_{lj}$, which coincides with the integration limits from the second integral of eq 65. Now if $\lambda_{lj} \leq |r - t| \leq a_{lj}$, and $t < r$, according to eq 64, we have that $r - \lambda_{lj} \geq t \geq r - a_{lj}$, which coincides with integration limits of the first integral.

(ii) $\Lambda_1^{(b)}(r)$ is defined only for $t > r$, i.e.,

$$\Lambda_1^{(b)}(r) \equiv \rho_l \int_{r}^{a_{\gamma l}} [-1][K_{lj}^1(r,t) + L_{lj}^1(r,t)]t\ dt \quad (66)$$

For $t > r$, and since $t_{max} < (r + \lambda_{lj})$, $(r + \lambda_{lj})$ is the upper and lower limit in the inequalities given by eqs 63 and 64, respectively, and the upper limit in the integral of $\Lambda_1^{(b)}(r)$ is $t_{max} \equiv a_{\gamma l}$; the kernels $L_{ij}^2(r,t)$ and $K_{ij}^2(r,t)$ are not defined, for $t > r$ (see eqs 64,60, and 61).

Thus, so far we have calculated $A_{lj}(r)$ only for $r \in [a_{\gamma j}, a_{\gamma l}]$, i.e., we still need to calculate the remainder of the interval $r \in [r_{min}, r_{max}] = [a_{\gamma j}, a_l + a_{\gamma j}]$, i.e, for $r \in [a_{\gamma l}, r_{max}]$. This interval is

$$\Lambda_1 \equiv \rho_l \int_{t_{min}}^{t_{max}} h_{\gamma l}(t)[L_{lj}(r,t) + K_{lj}(r,t)]t\ dt, \quad \text{where } r \in [a_{gj}, a_{gl}]t\ dt \quad (67)$$

Performing the integrals indicated in eq 67, we obtain the following analytical expression for $\Lambda_1(r)$:

$$\Lambda_1(r) = -\left[\frac{1}{r}\right]\cdot[\rho_l(o_{lj} + b_{lj} + e_{lj} + w_{lj} + x_{lj} + y_{lj})] \quad (68)$$

such that

$$o_{lj} \equiv \frac{\beta q_l q_j}{\varepsilon}\left[-\frac{1}{6}r^3 - \frac{1}{2}\lambda_{lj}r^2 + \frac{1}{2}(\lambda_{lj}^2 + a_{\gamma l}^2)r - \frac{1}{3}a_{\gamma l}^3 - \frac{1}{6}\lambda_{lj}^3 + \frac{1}{2}\lambda_{lj}a_{\gamma l}^2\right] \quad (69)$$

$$b_{lj} \equiv \left[\frac{\beta e^2 \omega_{lj}}{\varepsilon} + U_l\right]\cdot\left[\frac{1}{24}r^4 - \frac{1}{4}(\lambda_{lj}^2 + a_{\gamma l}^2)r^2 + \frac{1}{3}(\lambda_{lj}^3 + a_{\gamma l}^3)r - \frac{1}{8}\lambda_{lj}^4 + \frac{1}{4}\lambda_{lj}^2 a_{\gamma l}^2 - \frac{1}{8}a_{\gamma l}^4\right] \quad (70)$$

$$e_{lj} \equiv \left[\frac{\beta e^2}{\varepsilon}\left(O_{lj} + \frac{q_l q_j}{e^2} + X_{lj}(0)\right) + U_l\right]\cdot \left[\frac{1}{3}a_{lj}^3 + \frac{1}{2}(\lambda_{lj} - a_{lj})r^2 + \frac{1}{2}(a_{lj}^2 - \lambda_{lj}^2)r - \frac{1}{3}\lambda_{lj}^3 + \frac{1}{2}(a_{lj} - \lambda_{lj})(a_{\gamma j}^2 - \lambda_{lj}^2) + \frac{1}{2}a_{lj}(\lambda_{lj}^2 - a_{lj}^2)\right] \quad (71)$$

$$w_{lj} \equiv \left[\frac{\beta e^2 P_{lj}}{\varepsilon} + U_{lj}\right]\cdot\left[\frac{1}{4}(\lambda_{lj}^2 - a_{lj}^2)r^2 + \frac{1}{3}(a_{lj}^3 - \lambda_{lj}^3)r - \frac{1}{8}\lambda_{lj}^4 + \frac{1}{8}a_{lj}^4 + \frac{1}{4}(a_{lj}^2 - \lambda_{lj}^2)(a_{\gamma l}^2 - \lambda_{lj}^2) + \frac{1}{4}a_{lj}^2(\lambda_{lj}^2 - a_{lj}^2)\right] \quad (72)$$

$$x_{lj} \equiv \left[\frac{\beta e^2 Q_{lj}}{\varepsilon} + T_{lj}\right]\cdot\left[\frac{1}{6}(\lambda_{lj}^3 - a_{lj}^3)r^2 - \frac{1}{15}\lambda_{lj}^5 + \frac{1}{15}a_{lj}^5 + \frac{1}{4}(a_{lj}^4 - \lambda_{lj}^4)r + \frac{1}{6}a_{lj}^3(\lambda_{lj}^2 - a_{lj}^2) + \frac{1}{6}(a_{lj}^3 - \lambda_{lj}^3)(a_{\gamma l}^3 - \lambda_{lj}^3)(a_{\gamma l}^2 - \lambda_{lj}^2)\right] \quad (73)$$

$$y_{lj} \equiv \left[\frac{\beta e^2 R_{lj}}{\varepsilon} + W\right]\cdot\left[\frac{1}{10}(\lambda_{lj}^5 - a_{lj}^5)r^2 + \frac{1}{6}(a_{lj}^6 - \lambda_{lj})r - \frac{1}{35}\lambda_{lj}^7 + \frac{1}{10}a_{lj}^5(\lambda_{lj}^2 - a_{lj}^2) + \frac{1}{35}a_{lj}^7 + \frac{1}{10}(a_{lj}^5 - \lambda_{lj}^5)(a_{\gamma l}^2 - \lambda_{lj}^2)\right] \quad (74)$$

Now is necessary to consider separately the $r \in (a_{\gamma l}, a_{\gamma l} + \lambda_{lj}]$ interval, since, for $t < r$ and $r > t_{max} = a_{\gamma l}$, the inequalities of eqs 63 and 64 are only satisfied for part of the $r \geq t \geq r - \lambda_{lj}$ interval, i.e., for $t_{max} = a_{\gamma l} = t \geq r - \lambda_{lj}$. These conditions over r and t only apply for $K_{ij}^1(r,t)$ and $L_{ij}^1(r,t)$. Additionally, for $K_{ij}^2(r,t)$ and $L_{ij}^2(r,t)$ the corresponding interval is $r - \lambda_{lj} \geq t \geq r - a_{lj}$. If we consider values above this interval of r, i.e., $r > a_{\gamma l} + \lambda_{lj}$, then the functions $K_{ij}^1(r,t)$ and $L_{ij}^1(r,t)$, are not defined, since necessarily $r - \lambda_{lj} \geq t_{max}$, and hence the inequality, $r \geq t \geq r - \lambda_{lj}$, cannot be satisfied. Therefore, defining a new $\Lambda_2(r)$ function for this interval, i.e., $r \in (a_{\gamma l}, a_{\gamma l} + \lambda_{lj}]$, we have

$$\Lambda_2(r) \equiv \rho_l \int_{r-a_{lj}}^{r-\lambda_{lj}} [-1][K_{lj}^2(r,t) + L_{lj}^2(r,t)]t\ dt + \rho_l \int_{r-\lambda_{lj}}^{a_{\gamma l}} [-1][K_{lj}^1(r,t) + L_{lj}^1(r,t)]t\ dt \quad (75)$$

and we find the analytical expression:

$$\Lambda_2(r) = -\left[\frac{1}{r}\right]\cdot[\rho_l(o_{lj} + b_{lj} + e_{lj} + w_{lj} + x_{lj} + y_{lj})] \quad (76)$$

where

$$o_{lj} \equiv \frac{\beta q_l q_j}{\varepsilon}\left[\frac{1}{6}r^3 - \frac{1}{2}\lambda_{lj}r^2 + \frac{1}{2}(\lambda_{lj}^2 - a_{\gamma l}^2)r + \frac{1}{3}a_{\gamma l}^3 - \frac{1}{6}\lambda_{lj}^3 + \frac{1}{2}\lambda_{lj}a_{\gamma l}^2\right] \quad (77)$$

$$b_{lj} \equiv \left[\frac{\beta e^2 \omega_{lj}}{\varepsilon} + U_l\right]\cdot\left[\frac{1}{24}r^4 - \frac{1}{4}(\lambda_{lj}^2 + a_{\gamma l}^2)r^2 + \frac{1}{3}(\lambda_{lj}^3 + a_{\gamma l}^3)r - \frac{1}{8}\lambda_{lj}^4 + \frac{1}{4}\lambda_{lj}^2 a_{\gamma l}^2 - \frac{1}{8}a_{\gamma l}^4\right] \quad (78)$$

All other functions e_{lj}, w_{lj}, x_{lj}, and y_{lj} are identical to the corresponding functions from the previous case.

dx.doi.org/10.1021/jp403313k | J. Phys. Chem. B 2013, 117, 11812−11829

Following this procedure, for the last interval, $r \in [a_{\gamma l} + \lambda_{lj}, a_{\gamma l} + a_l]$, and defining a function $\Lambda_3(r)$ for this interval, i.e.,

$$\Lambda_3(r) \equiv \rho_l \int_{r-\lambda_{lj}}^{a_{\gamma l}} [-1][K_{lj}^2(r, t) + L_{lj}^2(r, t)]t \, dt \tag{79}$$

Hence,

$$\Lambda_3(r) = -\left[\frac{1}{r}\right]\cdot[\rho_l(e_{lj} + w_{lj} + x_{lj} + y_{lj})] \tag{80}$$

where

$$e_{lj} \equiv \left[\frac{\beta e^2}{\varepsilon}\left(O_{lj} + \frac{q_l q_j}{e^2} + X_{lj}(0)\right) + U_l\right]\cdot \left[\frac{1}{6}r^3 - \frac{1}{2}a_{lj}r^2 + \frac{1}{2}(a_{lj}^2 - a_{\gamma j}^2)r + \frac{1}{3}a_{\gamma j}^3 + \frac{1}{3}a_{lj}^3 + \frac{1}{2}a_{lj}(a_{\gamma j}^2 - a_{lj}^2)\right] \tag{81}$$

$$w_{lj} \equiv \left[\frac{\beta e^2 P_{lj}}{\varepsilon} + U_{lj}\right]\cdot\left[\frac{1}{24}r^4 - \frac{1}{4}(a_{\gamma j}^2 + a_{lj}^2)r^2 + \frac{1}{3}(a_{lj}^3 + a_{\gamma j}^3)r - \frac{1}{8}a_{\gamma j}^4 + \frac{1}{8}a_{lj}^4 + \frac{1}{4}a_{lj}^2(a_{\gamma j}^2 - a_{lj}^2)\right] \tag{82}$$

$$x_{lj} \equiv \left[\frac{\beta e^2 Q_{lj}}{\varepsilon} + T_{lj}\right]\cdot\left[\frac{1}{60}r^5 - \frac{1}{6}a_{\gamma j}^2 r^3 + \frac{1}{3}\left(a_{\gamma j}^3 - \frac{1}{2}a_{lj}^3\right)r^2 + \frac{1}{4}(a_{lj}^4 - a_{\gamma j}^4)r + \frac{1}{15}a_{\gamma j}^5\frac{1}{15}a_{\gamma j}^5 + \frac{1}{6}a_{lj}^3(a_{lj}^2 - a_{\gamma j}^2)\right] \tag{83}$$

$$y_{lj} \equiv \left[\frac{\beta e^2 R_{lj}}{\varepsilon} + W\right]\cdot\left[\frac{1}{210}r^7 - \frac{1}{10}a_{\gamma j}^2 r^5 + \frac{1}{3}a_{\gamma j}^3 r^4 - \frac{1}{2}a_{\gamma j}^4 r^3 + \frac{1}{5}\left(2a_{\gamma j}^5 - \frac{1}{2}a_{lj}^5\right)r^2 + \frac{1}{6}(a_{lj}^6 - a_{\gamma j}^6)r + \frac{1}{35}a_{\gamma j}^7 + \frac{1}{35}a_{lj}^7 + \frac{1}{10}(a_{\gamma j}^2 - a_{lj}^2)\right] \tag{84}$$

Thus, for $a_l > a_j$, $A_{lj}(r) = \Lambda_1(r) + \Lambda_2(r) + \Lambda_3(r)$.

2. **The $A_{lj}(r)$ function, when $a_l < a_j$.** For this case, $A_{lj}(r) = \Lambda_3(r)$, which has been computed above (see eq 80).

3. **The $A_{lj}(r)$ function, when $a_l = a_j$.**

For this case,

$$A_{lj}(r) = \rho_l c_1\left(\frac{1}{24}r^4 - \frac{1}{4}(a_{lj}^2 + a_{\gamma j}^2)r^2 + \frac{1}{3}(a_{lj}^3 + a_{\gamma j}^3)r - \frac{1}{8}a_{\gamma j}^4 + \frac{1}{8}a_{lj}^4 + \frac{a_{lj}^2}{4}(a_{\gamma j}^2 - a_{lj}^2)\right) + 6\eta c_2\sum_{l=1}^{j}\rho_l\left[\frac{1}{60}r^5 - \frac{1}{60}a_{\gamma l}^2 r^3 + \frac{1}{3}\left(a_{\gamma l}^3 - \frac{1}{2}a_{lj}^3\right)r^2 + \frac{1}{4}(a_{lj}^4 - a_{\gamma l}^4)r + \frac{1}{15}a_{\gamma l}^5 + \frac{1}{15}a_{lj}^5 + \frac{a_{lj}^3}{6}(a_{\gamma l}^2 - a_{lj}^2)\right] + \sum_{l=1}^{j}\rho_l\frac{\eta c_3}{2}\left[\frac{1}{210}r^7 - \frac{1}{10}a_{\gamma l}^2 r^5 + \frac{1}{3}a_{\gamma l}^3 r^4 - \frac{1}{2}a_{\gamma l}^4 r^3 + \left(-\frac{1}{10}a_{lj}^5 + \frac{2}{5}a_{\gamma l}^5\right)r^2 + \left(\frac{1}{6}a_{lj}^6 - \frac{1}{6}a_{\gamma l}^6\right)r + \frac{1}{35}a_{\gamma l}^7 + \frac{1}{35}a_{\gamma l}^7 + \frac{1}{35}a_{lj}^7\frac{a_{lj}^3}{6}(a_{\gamma l}^2 - a_{lj}^2)\right] \tag{85}$$

where

$$c_1 = \frac{(1 + 2\eta)^2}{(1 - \eta)^4} \tag{86}$$

$$c_2 = -\frac{(1 + \eta/2)^2}{a_l(1 - \eta)^4} \tag{87}$$

$$c_3 = \frac{c_1}{a_l^3} \tag{88}$$

$$\eta = \frac{\pi a_j^3\sum_{l=1}^{4}}{6} \tag{89}$$

Finally, we have shown that eq 16 is analytically given by

$$A_j(r) = \sum_{l=M,+,-,c} A_{lj}(r) \tag{90}$$

where each $A_{lj}(r)$ depends on the size relation between the different sizes of the l and j species.

APPENDIX B: THE MEAN ELECTROSTATIC POTENTIAL

Given an arbitrary density distribution of electrical charges, $\rho_{el}(\mathbf{y})$, where $\mathbf{y}$ is the position vector of the charges, the electrostatic potential, $\phi(\mathbf{r})$, at an arbitrary position $\mathbf{r}$, with respect to the charge distribution, in **SI** units, is given by[100]

$$\phi(\mathbf{r}) = \frac{1}{\varepsilon}\int_V \frac{\rho_{el}(y)d^3y}{|\mathbf{r} - \mathbf{y}|} \tag{91}$$

where ε is the dielectric constant of the dielectric media. $\phi(\mathbf{r})$ is the electrostatic potential energy necessary to bring a test particle, from infinity to a position $\mathbf{r}$, with respect to the charge distribution.

In a charged fluid, say a colloidal dispersion, with a charge distribution, $\rho_{el}(y)$, given by eq 23, the mean electrostatic potential, $\psi(r)$, at a distance $r \equiv |\mathbf{r}|$ from the central particle, of species γ, diameter a_γ, and surface charge density σ_γ, is given by

dx.doi.org/10.1021/jp403313k | J. Phys. Chem. B 2013, 117, 11812−11829

$$\psi(r) = \frac{1}{\varepsilon}\int_V \frac{\rho_{el}(y)d^3y}{|\mathbf{r}-\mathbf{y}|} \tag{92}$$

where we have taken into account the system's spherical symmetry, defined as $y \equiv |\mathbf{y}|$, and where the vectors $\mathbf{r}$ and $\mathbf{y}$ refer to the observation point and the charge location in the charge distribution, respectively. The charge distribution, $\rho_{el}(y)$, in terms of radial distribution functions, is given by (see eq 23)

$$\rho_{el}(y) = \sigma_\gamma \delta\left(y - \frac{a_\gamma}{2}\right) + \sum_{l=M,+,-,c} q_l \rho_l g_{\gamma l}(y) \tag{93}$$

Substituting eq 93 in eq 92, with the variable change $s \equiv |\mathbf{r}-\mathbf{y}| = [r^2 - 2ry\cos\theta + y^2]^{1/2}$, where the corresponding volume element is $d^3y = (ys/r)\,dy\,ds\,d\phi$, i.e., since $s^2 = r^2 - 2ry\cos\theta + y^2$, which implies that $\sin\theta\,d\theta = (s\,ds)/ry$, we get

$$\psi(r) = I_1(r) + I_2(r) \tag{94}$$

where we have defined

$$I_1(r) \equiv \frac{2\pi}{\varepsilon}\int_0^\infty \left(\frac{y}{r}\right)\sigma_\gamma \delta\left(y - \frac{a_\gamma}{2}\right) dy \int_{|r-y|}^{|r+y|} ds \tag{95}$$

and

$$I_2(r) \equiv \frac{2\pi}{\varepsilon}\sum_{l=M,+,-,c}\int_0^\infty \left(\frac{y}{r}\right) q_l\rho_l g_{\gamma l}(y)\,dy \int_{|r-y|}^{|r+y|} ds \tag{96}$$

More explicitly,

$$I_1(r) = I_1^a(r) + I_1^b(r) = \begin{cases} I_1^a(r) = \dfrac{2\pi}{\varepsilon}\displaystyle\int_0^r \left(\frac{y}{r}\right)\sigma_\gamma\delta\left(y-\frac{a_\gamma}{2}\right) \\ \quad [r+y-(r-y)]\,dy, \quad \text{for } r > y \\ I_1^b(r) = \dfrac{2\pi}{\varepsilon}\displaystyle\int_r^\infty \left(\frac{y}{r}\right)\sigma_\gamma\delta\left(y-\frac{a_{\gamma l}}{2}\right) \\ \quad [r+y-(y-r)]\,dy, \quad \text{for } r < y \end{cases} \tag{97}$$

and

$$I_2(r) = I_2^a(r) + I_2^b(r) = \begin{cases} I_2^a(r) = \dfrac{2\pi}{\varepsilon}\displaystyle\sum_{l=M,+,-,c}\int_{a_{\gamma 1}}^r \left(\frac{y}{r}\right) q_l\rho_l g_{\gamma l}(y) \\ \quad [r+y-(r-y)]\,dy, \quad \text{for } r > y \\ I_2^b(r) = \dfrac{2\pi}{\varepsilon}\displaystyle\sum_{l=M,+,-,c}\int_r^\infty \left(\frac{y}{r}\right) q_l\rho_l g_{\gamma l}(y) \\ \quad [r+y-(y-r)]\,dy, \quad \text{for } r < y \end{cases} \tag{98}$$

Considering that the r-vector points outside of the central particle, the second integral in eq 97, for $y > r > a_{\gamma l}/2$, implies that, $\delta(y - a_{\gamma l}/2) = 0$. Hence, this integral will always be zero for $y > r$, and, thus, $I_1(r)$ reduces to

$$I_1(r) = \frac{\pi\sigma_\gamma a_\gamma^2}{\varepsilon r} \tag{99}$$

where, by electroneutrality (see eq 21),

$$\sigma_\gamma = -\frac{4}{(a_\gamma)^2}\sum_{l=M,+,-,c}\int_{a_{\gamma 1}}^\infty q_l\rho_l g_{\gamma l}(y)y^2\,dy \tag{100}$$

The lower limit in this integral ($a_{\gamma 1} \equiv (a_\gamma + a_1)/2$) is because the distribution of the particles begins at the contact position of the central particle with a particle of species $i = 1$, which we have chosen to have the smallest diameter, a_1. Then, substituting eq 100 in eq 99, we have

$$I_1(r) = -\frac{4\pi}{\varepsilon}\sum_{l=M,+,-,c}\int_{a_{\gamma 1}}^\infty q_l\rho_l g_{\gamma l}(y)\frac{y^2}{r}\,dy \tag{101}$$

which can be split as

$$I_1(r) = -\frac{4\pi}{\varepsilon}\sum_{l=M,+,-,c}\int_{a_{\gamma 1}}^r q_l\rho_l g_{\gamma l}(y)\frac{y^2}{r}\,dy - \frac{4\pi}{\varepsilon}\sum_{l=M,+,-,c}\int_r^\infty q_l\rho_l g_{\gamma l}(y)\frac{y^2}{r}\,dy \tag{102}$$

Note that first integral (left) from this equation is the same as the $I_2^a(r)$-integral in eq 98, such that $\psi(r) = I_1(r) + I_2(r)$ is reduced to

$$\psi(r) = \frac{4\pi}{\varepsilon}\sum_{l=M,+,-,c}\int_r^\infty q_l\rho_l g_{\gamma l}(y)\left(y - \frac{y^2}{r}\right)dy \tag{103}$$

This is the mean electrostatic potential in terms of radial distribution function. However, since (see eq 14)

$$\rho_{el}(y) = \sum_{l=M,+,-,c} q_l\rho_l g_{\gamma l}(y) \tag{104}$$

eq 103 can also be expressed in terms of the charge concentration profile, $\rho_{el}(y)$, as

$$\psi(r) = \frac{4\pi}{\varepsilon}\int_r^\infty \rho_{el}(y)\left(y - \frac{y^2}{r}\right)dy \tag{105}$$

which is eq 13. In this derivation we have not assumed any particular charge distribution on the colloid particles, and, hence it can be applied to the CPM or the MCPM. Equation 103 is a general expression for the electrostatic potential, $\psi(r)$, due to an arbitrary charge distribution, $\rho_{el}(y)$. In fact, eq 105 is the general solution of the Poisson equation in spherical coordinates, i.e.,

$$\nabla^2\psi(r) = \frac{4\pi}{\varepsilon}\rho_{el}(y) \tag{106}$$

for an arbitrary charge distribution.

Hence, if in eq 103 (or eq 13) we use eq 23, together with eq 25, we obtain the mean electrostatic potential for the CPM model, but if we take eq 23 with eq 25, we obtain the mean electrostatic potential for the MCPM. To derive eq 12, we observe that $I_1(r)$ can be written as

$$I_1(r) = \frac{4\pi}{\varepsilon}\frac{(a_\gamma/2)^2}{r}\sigma_\gamma \tag{107}$$

which, in terms of electrostatic potential energy ($u_{\gamma j}$), between j and γ, is

$$I_1(r) = \frac{u_{\gamma j}(r)}{q_j} \tag{108}$$

Since the fluid is electroneutral, i.e.,

dx.doi.org/10.1021/jp403313k | J. Phys. Chem. B 2013, 117, 11812−11829

$$\sum_{l=1}^{4} q_l \rho_l = 0 \tag{109}$$

subtracting eq 109 from eq 96, we get

$$I_2(r) \equiv \frac{2\pi}{\varepsilon} \sum_{l=M,+,-,c} \int_{a_{\gamma l}}^{\infty} \left(\frac{y}{r}\right) q_l \rho_l [g_{\gamma 1}(y) - 1]\, dy \int_{r-y}^{r+y} ds \tag{110}$$

Remembering that $h_{\gamma 1} \equiv g_{\gamma 1}(y) - 1$, and considering eq 98, we have that eq 110 can be written as

$$I_2(r) = -\frac{2\pi}{r}\left(\frac{1}{\varepsilon}\right) \sum_{l=M,+,-,c} \int_{a_{\gamma 1}}^{\infty} q_l \rho_l h_{\gamma l}(y) f_1(r, y) y\, dy \tag{111}$$

where $f_1(r,y) \equiv -[r + y - |r - y|]$. Thus, the corresponding mean electrostatic potential, given by eq 12, is

$$\psi(r) = \frac{u_{\gamma j}(r)}{q_j} - \frac{2\pi}{r}\left(\frac{1}{\varepsilon}\right) \sum_{l=M,+,-,c} \int_{a_{\gamma 1}}^{\infty} q_l \rho_l h_{\gamma l}(y) f_1(r, y) y\, dy \tag{112}$$

Equations 112 and 103 are equivalent.

AUTHOR INFORMATION

Corresponding Author

*E-mail: marcelo@imp.mx; Phone: 0155-91756402.

Notes

The authors declare no competing financial interest.

ACKNOWLEDGMENTS

The support of CONACYT (Grant No. 169125) is gratefully acknowledged.

REFERENCES

(1) Verwey, E. J. W.; Overbeek, J. T. G. *Theory of the Stability of Lyophobic Colloids*; Dover: New York, 1948.

(2) McQuarrie, D. A. *Statistical Mechanics*; Harper and Row: New York, 1976.

(3) Medina-Noyola, M.; McQuarrie, D. An Extended Mean Spherical Approximation for Coulombic Systems. *J. Chem. Phys.* **1981**, *74*, 3025−3032.

(4) Torrie, G. M.; Valleau, J. P. Electrical Double-Layers. I. Monte-Carlo Study of a Uniformly Charged Surface. *J. Chem. Phys.* **1980**, *73*, 5807−5816.

(5) Valleau, J. P.; Ivkov, R.; Torrie, G. M. Colloid Stability: The Forces between Charged Surfaces in an Electrolyte. *J. Chem. Phys.* **1991**, *95*, 520−532.

(6) Belloni, L. Colloidal Interactions. *J. Phys.: Condens. Matter* **2000**, *12*, R549−R587.

(7) Stillinger, F. H.; Kirkwood, J. G. Theory of the Diffuse Double Layer. *J. Chem. Phys.* **1960**, *33*, 1282−1290.

(8) Croxton, T. L.; McQuarrie, D. Numerical-Solution of the Born-Green-Ivon Equation for the Restricted Primitive Model of Ionic-Solutions. *J. Phys. Chem.* **1979**, *83*, 1840−1843.

(9) Outhwaite, C. W.; Bhuiyan, L. B. An Improved Modified Poisson-Boltzmann Equation in Electric Double Layer Theory. *J. Chem. Soc., Faraday Trans. 2* **1983**, *79*, 707.

(10) Outhwaite, C. W.; Bhuiyan, L. B. A Modified Poisson-Boltzmann Equation in Electric Double Layer Theory for a Primitive Model Electrolyte with Size-Asymmetric Ions. *J. Chem. Phys.* **1986**, *84*, 3461−3471.

(11) Grimson, M. J.; Rickayzen, G.; Richmond, P. Short Range Solvation Forces in Fluids I. General Formalism and Hard Particle Fluids. *Mol. Phys.* **1980**, *39*, 61−73.

(12) Grimson, M. J.; Rickayzen, G. Solvation Forces in Charged Fluids. *Mol. Phys.* **1981**, *44*, 817−840.

(13) Evans, R. In *Density Functionals in the Theory of Nonuniform Fluids*; Fundamentals of Inhomogeneous Fluds; Marcel Dekker: New York, 1992; Chapter 3.

(14) Patey, G. N. The Interaction of Two Spherical Colloidal Particles in Electrolyte Solution. An Application of the Hypernetted-Chain Approximation. *J. Chem. Phys.* **1980**, *72*, 5763−5770.

(15) Lozada-Cassou, M. The Force between Two Planar Electrical Double Layers. *J. Chem. Phys.* **1984**, *80*, 3344−3349.

(16) Nielaba, P.; Fortsmann, F. Packing of Ions Near an Electrolyte−Electrode Interface in the HNC/LMSA Approximation to the RPM Model. *Chem. Phys. Lett.* **1985**, *117*, 46−48.

(17) Kjellander, R.; Marčelja, S. Inhomogeneous Coulomb Fluids with Image Interactions between Planar Surfaces. I. *J. Chem. Phys.* **1985**, *82*, 2122−2135.

(18) Kjellander, R.; Marčelja, S. Interaction of Charged Surfaces in Electrolyte Solutions. *Chem. Phys. Lett.* **1986**, *127*, 402−407.

(19) Plischke, M.; Henderson, D. Pair and Singlet Correlation Functions of Inhomogeneous Fluids Calculated Using Ornstein-Zernike Equations. *J. Phys. Chem.* **1988**, *92*, 7177−7185.

(20) Sánchez, J.; Lozada-Cassou, M. Exact Numerical Solution to the Integral Equation Version of the Poisson-Boltzmann Equation for Two Interacting Spherical Particles. *Chem. Phys. Lett.* **1992**, *190*, 202−208.

(21) Lozada-Cassou, M. In *Fluids between Walls and in Pores*; *Fundamentals of Inhomogeneous Fluds*; Marcel Dekker: New York, 1992; Chapter 8.

(22) Attard, P. Electrolytes and the Electric Double Layer. In *Advances in Chemical Physics*; Prigogine, I., Rice, S. A., Eds.; John Wiley and Sons, Inc.: New York, 1996; Vol. *XCII*.

(23) González-Tovar, E.; Lozada-Cassou, M.; Henderson, D. Hypernetted Chain Approximation for the Distribution of Ions around a Cylindrical Electrode. II. Numerical Solution for a Model Cylindrical Polyelectrolyte. *J. Chem. Phys.* **1985**, *83*, 361−373.

(24) Lozada-Cassou, M.; Henderson, D. The Force between Two Planar Electrical Double Layers: Some Numerical Results. *Chem. Phys. Lett.* **1986**, *127*, 392−397.

(25) González-Tovar, E.; Lozada-Cassou, M. The Spherical Double-Layer: A Hypernetted Chain Mean Spherical Approximation Calculation for a Model Spherical Colloid Particle. *J. Chem. Phys.* **1989**, *93*, 3761−3768.

(26) Jiménez-Ángeles, F.; Messina, R.; Holm, C.; Lozada-Cassou, M. Ion Pairing in Model Electrolytes: A Study via Three-Particle Correlation Functions. *J. Chem. Phys.* **2003**, *119*, 4842−4856.

(27) Jiménez-Ángeles, F.; Odriozola, G.; Lozada-Cassou, M. Electrolyte Distribution around Two Like-Charged Rods: Their Effective Attractive Interaction and Angular Dependent Charge Reversal. *J. Chem. Phys.* **2006**, *124*, 134902(1)−134902(18).

(28) Guerrero-García, G. I.; González-Tovar, E.; Lozada-Cassou, M.; de J. Guevara-Rodríguez, F. The Electrical Double Layer for a Fully Asymmetric Electrolyte around a Spherical Colloid: An Integral Equation Study. *J. Chem. Phys.* **2005**, *123*, 034703(1)−034703(20).

(29) Lozada-Cassou, M.; Díaz-Herrera, E. The Application of the Hypernetted Chain Approximation to the Electrical Double-Layer: Comparison with Monte-Carlo Results for Symmetric Salts. *J. Chem. Phys.* **1982**, *77*, 5150−5156.

(30) Greberg, H.; Kjellander, R. Charge Inversion in Electric Double Layers and Effects of Different Sizes for Counterions and Coions. *J. Chem. Phys.* **1998**, *108*, 2940−2953.

(31) Wernersson, E.; Kjellander, R.; Lyklema, J. Charge Inversion and Ion−Ion Correlation Effects at the Mercury/Aqueous $MgSO_4$ Interface: Toward the Solution of a Long-Standing Issue. *J. Phys. Chem. C* **2010**, *114*, 1849−1866.

(32) Lozada-Cassou, M. Hypernetted Chain Theory for the Distribution of Ions around a Cylindrical Electrode. *J. Phys. Chem.* **1983**, *87*, 3729−3732.

(33) Elimelech, M.; O'Melia, C. R. Effect of Electrolyte Type on the Electrophoretic Mobility of Polystyrene Latex Colloids. *Colloids Surf.* **1990**, *44*, 165−178.

(34) Lozada-Cassou, M.; González-Tovar, E.; Olivares, W. Nonlinear Effects in the Electrophoresis of a Spherical Colloidal Particle. *Phys. Rev. E* **1999**, *60*, R17−R20.
(35) Shklovskii, B. I. Screening of a Macroion by Multivalent Ions: Correlation-Induced Inversion of Charge. *Phys. Rev. E* **1999**, *60*, 5802−5811.
(36) Nguyen, T. T.; Grosberg, A. Y.; Shklovskii, B. I. Macroions in Salty Water with Multivalent Ions: Giant Inversion of Charge. *Phys. Rev. Lett.* **2000**, *85*, 1568−1571.
(37) Lozada-Cassou, M.; González-Tovar, E. Primitive Model Electrophoresis. *J. Colloid Interface Sci.* **2001**, *239*, 285−295.
(38) Lozada-Cassou, M.; González-Tovar, E. ERRATUM Primitive Model Electrophoresis. *J. Colloid Interface Sci.* **2001**, *240*, 644−644.
(39) Tanaka, M. Effects of Asymmetric Salt and A Cylindrical Macroion on Charge Inversion: Electrophoresis by Molecular Dynamics Simulations. *Phys. Rev. E* **2003**, *68*, 061501(1)−061501(8).
(40) Quesada-Pérez, M.; González-Tovar, E.; Martín-Molina, A.; Lozada-Cassou, M.; Hidalgo-Álvarez, R. Overcharging in Colloids: Beyond the Poisson-Boltzmann Approach. *Chem. Phys. Chem* **2003**, *4*, 234−248.
(41) Martín-Molina, A.; Quesada-Pérez, M.; Galisteo-González, F.; Hidalgo-Álvarez, R. Looking into Overcharging in Model Colloids through Electrophoresis: Asymmetric Electrolytes. *J. Chem. Phys.* **2003**, *118*, 4183−4189.
(42) Besteman, K.; Eijk, K. V.; Lemay, S. G. Charge Inversion Accompanies DNA Condensation by Multivalent Ions. *Nat. Phys.* **2007**, *3*, 641−644.
(43) Lobaskin, V.; Dünweg, B.; Medebach, M.; Palberg, T.; Holm, C. Electrophoresis of Colloidal Dispersions in the Low-Salt Regime. *Phys. Rev. Lett.* **2007**, *98*, 176105(1)−176105(4).
(44) Lenz, O.; Holm, C. Simulation of Charge Reversal in Salty Environments: Giant Overcharging? *Eur. Phys. J. E* **2008**, *26*, 191−195.
(45) Diehl, A.; Levin, Y. Colloidal Charge Reversal: Dependence on the Ionic Size and the Electrolyte Concentration. *J. Chem. Phys.* **2008**, *129*, 124506(1)−124506(5).
(46) Martín-Molina, A.; Rodríguez-Beas, C.; Faraudo, J. Charge Reversal in Anionic Liposomes: Experimental Demonstration and Molecular Origin. *Phys. Rev. Lett.* **2010**, *104*, 168103(1)−168103(4).
(47) Sogami, I.; Ise, N. On the Electrostatic Interaction in Macroion Solutions. *J. Chem. Phys.* **1984**, *81*, 6320−6332.
(48) Kjellander, R.; Marčelja, S. Correlation and Image Charge Effects in Electric Double Layers. *Chem. Phys. Lett.* **1984**, *112*, 49−53.
(49) Lozada-Cassou, M.; Díaz-Herrera, E. Three Point Extension for Hypernatted Chain and other Integral Equation Theories: Numerical Results. *J. Chem. Phys.* **1990**, *92*, 1194−1210.
(50) Allahyarov, E.; D'Amico, I.; Löwen, H. Attraction between Like-Charged Macroions by Coulomb Depletion. *Phys. Rev. Lett.* **1998**, *81*, 1334−1337.
(51) Diehl, A.; Tamashiro, M. N.; Barbosa, M. C.; Levin, Y. Density-Functional Theory for Attraction between Like-Charged Plates. *Physica A* **1999**, *274*, 433−445.
(52) Linse, P.; Lobaskin, V. Electrostatic Attraction and Phase Separation in Solutions of Like-Charged Colloidal Particles. *Phys. Rev. Lett.* **1999**, *83*, 4208−4211.
(53) Ariel, G.; Andelman, D. Persistence Length of a Strongly Charged Rodlike Polyelectrolyte in the Presence of Salt. *Phys. Rev. E* **2003**, *67*, 011805(1)−011805(11).
(54) Lobaskin, V.; Qamhieh, K. Effective Macroion Charge and Stability of Highly Asymmetric Electrolytes at Various Salt Conditions. *J. Phys. Chem. B* **2003**, *107*, 8022−8029.
(55) Jiménez-Ángeles, F.; Lozada-Cassou, M. A Model Macroion Solution Next to a Charged Wall: Overcharging, Charge Reversal, and Charge Inversion by Macroions. *J. Phys. Chem. B* **2004**, *108*, 7286−7296.
(56) Messina, R.; González-Tovar, E.; Lozada-Cassou, M.; Holm, C. Overcharging: The Crucial Role of Excluded Volume. *Europhys. Lett.* **2002**, *60*, 383−389.
(57) Wang, Z.-Y.; Ma, Y.-Q. Insights from Monte Carlo Simulations on Charge Inversion of Planar Electric Double Layers in Mixtures of Asymmetric Electrolytes. *J. Chem. Phys.* **2010**, *133*, 064704(1)−064704(10).
(58) Chialvo, A. A.; Simonson, J. M. On the Molecular Mechanism of Surface Charge Amplification and Related Phenomena at Aqueous Polyelectrolyte−Graphene Interfaces. *Condens. Matter Phys.* **2011**, *14*, 33002(1)−33002(10).
(59) In the literature, overcharging has been used, in the past, as a synonymous of charge reversal or charge inversion. However, this is an unfortunate used of the word overcharging, which is synonymous with overload.
(60) Guerrero-García, G. I.; González-Tovar, E.; Chávez-Páez, M.; Lozada-Cassou, M. Overcharging and Charge Reversal in the Electrical Double Layer around the Point of Zero Charge. *J. Chem. Phys.* **2010**, *132*, 054903(1)−054903(19).
(61) Yu, Y.-X.; Wu, J.; Gao, G.-H. Density-Functional Theory of Spherical Electric Double Layers and ζ Potentials of Colloidal Particles in Restricted-Primitive-Model Electrolyte Solutions. *J. Chem. Phys.* **2004**, *120*, 7223−7233.
(62) Manzanilla-Granados, H. M.; Jiménez-Ángeles, F.; Lozada-Cassou, M. The Zeta-Potential for a Concentrated Colloidal Dispersion: The Colloidal Primitive Model vs. the Cell Model. *Colloids Surf., A* **2011**, *376*, 59−66.
(63) Manzanilla-Granados, H. M.; Jiménez-Ángeles, F.; Lozada-Cassou, M. Polarity Inversion of Zeta-Potential in Concentrated Colloidal Dispersions. *J. Phys. Chem. B* **2011**, *115*, 12094−12097.
(64) Oshima, H. Electrophoretic Mobility of Spherical Colloidal Particles in Concentrated Suspensions. *J. Colloid Interface Sci.* **1997**, *188*, 481−485.
(65) Antypov, D.; Holm, C. Optimal Cell Approach to Osmotic Properties of Finite Stiff-Chain Polyelectrolytes. *Phys. Rev. Lett.* **2006**, *96*, 088302(1)−088302(4).
(66) Ruiz-Reina, E.; Carrique, F. Electric Double Layer of Spherical Particles in Salt-Free Concentrated Suspensions: Water Dissociation and CO_2 Influence. *J. Phys. Chem. B* **2008**, *112*, 11960−11967.
(67) Bret, M. L.; Zimm, B. H. Monte Carlo Determination of the Distribution of Ions About a Cylindrical Polyelectrolyte. *Biopolymers* **1984**, *23*, 271−285.
(68) Messina, R. Spherical Colloids: Effect of Discrete Macroion Charge Distribution and Counterion Valence. *Physica A* **2002**, *308*, 59−79.
(69) Kielland, J. Individual Activity Coefficients of Ions in Aqueous Solutions. *J. Am. Chem. Soc.* **1937**, *59*, 1675−1678.
(70) Israelachvili, J. N. *Intermolecular and Surface Forces*, 2nd ed.; Academic Press: New York, 1992.
(71) Ben-Yaakov, D.; Andelman, D.; Diamant, H. Interaction between Heterogeneously Charged Surfaces: Surface Patches and Charge Modulation. *Phys. Rev. E* **2013**, *87*, 022402(1)−022402(10).
(72) Lozada-Cassou, M. A New Method of Deriving Electrical Double Layer Equations from Electrolyte Theories. *J. Chem. Phys.* **1981**, *75*, 1412−1421.
(73) Hiroike, K. Ornstein-Zernike Relation for a Fluid Mixture with Direct Correlation Functions of Finite Range. *J. Phys, Soc. Jpn.* **1969**, *27*, 1415−1421.
(74) Blum, L. Mean Spherical Model for Asymmetric Electrolytes. I. Method of Solution. *Mol. Phys.* **1975**, *30*, 1529−1535.
(75) Hiroike, K. Suplement to Blum Theory for Asymmetric Electrolytes. *Mol. Phys.* **1977**, *33*, 1195−1198.
(76) MieryTerán, L.; Falls, A. H.; Scriven, L. E.; Davis, H. T. In MieryTerán, L.; Falls, A. H.; Scriven, L. E.; Davis, H. T.; Sengers, J. V., Ed.; American Society of Mechanical Engineers: New York, 1982; Vol. *I*.
(77) MieryTerán, L.; Díaz-Herrera, E.; Lozada-Cassou, M.; Henderson, D. Temperature Dependence of the Primitive-Model Double Layer Differential Capacitance: A Hypernetted Chain/Mean Spherical Approximation Calculation. *J. Phys. Chem.* **1988**, *92*, 6408−6413.
(78) Jiménez-Ángeles, F.; Lozada-Cassou, M. Simple Model for Semipermeable Membrane: Donnan Equilibrium. *J. Phys. Chem. B* **2004**, *108*, 1719−1730.

(79) Lozada-Cassou, M.; Díaz-Herrera, E. Three-Point Extension Hypernetted Chain, Conventional Hypernetted Chain, and Superposition Approximations: Numerical Results for the Force between Two Plates. *J. Chem. Phys.* **1990**, *93*, 1386−1398.
(80) Lozada-Cassou, M.; Olivares, W.; Sulbarán, B. Violation of the Electroneutrality Condition in Confined Charged Fluids. *Phys. Rev. E* **1996**, *53*, 522−530.
(81) Wu, J.; Bratko, D.; Prausnitz, J. M. Interaction between Like-Charged Colloidal Spheres in Electrolyte Solutions. *Proc. Natl. Acad. Sci. U.S.A.* **1998**, *95*, 15169−15172.
(82) Langmuir, I. The Role of Attractive and Repulsive Forces in the Formation of Tactoids, Thixotropic Gels, Protein Crystals and Coacervates. *J. Chem. Phys.* **1938**, *6*, 873−896.
(83) Ito, K.; Yoshida, H.; Ise, N. Void Structure in Colloidal Dispersions. *Science* **1994**, *263*, 66−68.
(84) Carbajal-Tinoco, M. D.; Castro-Román, F.; Arauz-Lara, J. L. Static Properties of Confined Colloidal Suspensions. *Phys. Rev. E* **1996**, *53*, 3745−3749.
(85) Schmitz, K. S. Volume-Term Theories, Sogami-Ise Potential, and Langmuir Model for Phase Separation in Macroion Systems: A Resolution. *Phys. Rev. E* **2002**, *65*, 061402(1)−061402(8).
(86) van Roij, R.; Hansen, J. P. van der Waals-Like Instability in Suspensions of Mutually Repelling Charged Colloids. *Phys. Rev. Lett.* **1997**, *79*, 3082−3085.
(87) van Roij, R.; Dijkstra, M.; Hansen, J. P. Phase Diagram of Charge-Stabilized Colloidal Suspensions: van der Waals Instability without Attractive Forces. *Phys. Rev. E* **1999**, *59*, 2010−2025.
(88) Warren, P. B. A Theory of Void Formation in Charge-Stabilized Colloidal Suspensions at Low Ionic Strength. *J. Chem. Phys.* **2000**, *112*, 4683−4698.
(89) Hunter, R. *Foundations of Colloid Science*; Oxford University Press: New York, 2001.
(90) Wiersema, P. H.; Loeb, A. L.; Overbeek, J. T. G. Calculation of the Electrophoretic Mobility of a Spherical Colloid Particle. *J. Colloid Interface Sci.* **1966**, *22*, 78−99.
(91) O'Brien, R. W.; White, L. R. Electrophoretic Mobility of a Spherical Colloidal Particle. *J. Chem. Soc., Faraday Trans. 2* **1978**, *74*, 1607−1626.
(92) Kosmulski, M. Zeta Potentials in Nonaqueous Media: How to Measure and Control Them. *Colloids Surf., A* **1999**, *159*, 277−281.
(93) Tanaka, M.; Grosberg, A. Y. Giant Charge Inversion of a Macroion due to Multivalent Counterions and Monovalent: Molecular Dynamic Study. *J. Chem. Phys.* **2001**, *115*, 567−574.
(94) Garbow, N.; Evers, M.; Palberg, T.; Okubo, T. On the Electrophoretic Mobility of Isolated Colloidal Spheres. *J. Phys.: Condens. Matter* **2004**, *16*, 3835−3842.
(95) Deserno, M.; Jiménez-Ángeles, F.; Holm, C.; Lozada-Cassou, M. Overcharging of DNA in the Presence of Salt: Theory and Simulation. *J. Phys. Chem. B* **2001**, *105*, 10983−10991.
(96) Evers, M.; Garbow, N.; Hessinger, D.; Palberg, T. Electrophoretic Mobility of Interacting Colloidal Spheres. *Phys. Rev. E* **1998**, *57*, 6774−6784.
(97) Palberg, T.; Medebach, M.; Garbow, N.; Evers, M.; Fontecha, A. B.; Reiber, H.; Bartsch, E. Electrophoresis of Model Colloidal Spheres in Low Salt Aqueous Suspension. *J. Phys.: Condens. Matter* **2004**, *16*, S4039−S4050.
(98) Medebach, M.; Palberg, T. Electrophoretic Mobility of Electrostatically Interacting Colloidal Spheres. *J. Phys.: Condens. Matter* **2004**, *16*, 5653−5658.
(99) Reiber, H.; Köller, T.; Palberg, T.; Carrique, F.; Reina, E. R.; Piazza, R. Salt Concentration and Particle Density Dependence of Electrophoretic Mobilities of Spherical Colloids in Aqueous Suspension. *J. Colloid Interface Sci.* **2007**, *309*, 315−322.
(100) Jackson, J. D. *Classical Electrodynamics*, 3rd ed.; John Wiley and Sons, Inc.: Hoboken, NJ, 1999.